

Research Paper

Mitochondrial Transfer from Bone Marrow Mesenchymal Stem Cells to Motor Neurons in Spinal Cord Injury Rats via Gap Junction

Heyangzi Li^{1*}, Chao Wang^{1*}, Teng He^{1*}, Tengfei Zhao², Ying-ying Chen¹, Yue-liang Shen¹, Xiaoming Zhang¹✉, Lin-lin Wang¹✉

1. Department of Basic Medicine Sciences, Zhejiang University School of Medicine, Hangzhou 310058, China

2. Department of Orthopedic Surgery, Second Affiliated Hospital of Zhejiang University School of Medicine, Hangzhou 310009, China

*These authors contributed equally to this work.

✉ Corresponding authors: Xiaoming Zhang, PhD, MD, Department of Basic Medicine Sciences, and Department of Emergency Medicine, Sir Run Run Shaw Hospital, Zhejiang University School of Medicine, Hangzhou, Zhejiang 310058, China. Tel and Fax: 0086-571-88208318; E-mail: zxm@zju.edu.cn and Lin-lin Wang, PhD, MD, Department of Basic Medicine Sciences, Zhejiang University School of Medicine, Hangzhou, Zhejiang 310058, China. Tel and Fax: 0086-571-88208250; E-mail: wanglinlin@zju.edu.cn

© Ivyspring International Publisher. This is an open access article distributed under the terms of the Creative Commons Attribution (CC BY-NC) license (<https://creativecommons.org/licenses/by-nc/4.0/>). See <http://ivyspring.com/terms> for full terms and conditions.

Received: 2018.08.22; Accepted: 2019.02.07; Published: 2019.03.17

Abstract

Recent studies have demonstrated that bone marrow mesenchymal stem cells (BMSCs) protect the injured neurons of spinal cord injury (SCI) from apoptosis while the underlying mechanism of the protective effect of BMSCs remains unclear. In this study, we found the transfer of mitochondria from BMSCs to injured motor neurons and detected the functional improvement after transplanting.

Methods: Primary rat BMSCs were co-cultured with oxygen-glucose deprivation (OGD) injured VSC4.1 motor neurons or primary cortical neurons. FACS analysis was used to detect the transfer of mitochondria from BMSCs to neurons. The bioenergetics profiling of neurons was detected by Extracellular Flux Analysis. Cell viability and apoptosis were also measured. BMSCs and isolated mitochondria were transplanted into SCI rats. TdT-mediated dUTP nick end labelling staining was used to detect apoptotic neurons in the ventral horn. Immunohistochemistry and Western blotting were used to measure protein expression. Re-myelination was examined by transmission electron microscope. BBB scores were used to assess locomotor function.

Results: MitoTracker-Red labelled mitochondria of BMSCs could be transferred to the OGD injured neurons. The gap junction intercellular communication (GJIC) potentiator retinoid acid increased the quantity of mitochondria transfer from BMSCs to neurons, while GJIC inhibitor 18 β glycyrrhetic acid decreased mitochondria transfer. Internalization of mitochondria improved the bioenergetics profile, decreased apoptosis and promoted cell survival in post-OGD motor neurons. Furthermore, both transplantation of mitochondria and BMSCs to the injured spinal cord improved locomotor functional recovery in SCI rats.

Conclusions: To our knowledge, this is the first evidence that BMSCs protect against SCI through GJIC to transfer mitochondrial to the injured neurons. Our findings suggested a new therapy strategy of mitochondria transfer for the patients with SCI.

Key words: spinal cord injury, bone marrow stromal cells, mitochondria, transfer, gap junction

Introduction

Spinal cord injury (SCI) that causes lifelong debilitation is characterized by an initial trauma and a secondary injury with vascular disruption [1], tissue ischaemia and hypoxia [2], oxidative stress [3], mitochondrial apoptosis [2], and axonal degeneration [4, 5]. Epidemiological data indicate that the incidence

of SCI is approximately 40.1 cases per million in the United States every year, and males are more likely experience SCI than females [6]. Recent studies have demonstrated that stem cell transplantation therapy offers an attractive alternative, especially for bone marrow mesenchymal stem cells (BMSCs) treatment

by secreting trophic factors, promoting axonal regeneration and improving neuron survival [7-9]. After SCI, the BMSCs have multiple effects on amelioration of immunomodulation and glial scarring [10, 11]. It may contribute to the integration of the graft with the host tissue and support the regeneration process [12]. However, the mechanism underlying the protection of BMSCs on SCI remains elusive.

Mitochondria is an important double-membraned organelle that produces energy through bio-oxidation in eukaryotic cells [13]. Under SCI conditions, the initial trauma that caused mitochondria disruption induces loss of adenosine triphosphate (ATP) synthesis and increases various reactive oxygen species (ROS) [14, 15]. The ability to restore mitochondria homeostasis and repair damaged mitochondria were beyond the neutralizing capabilities of antioxidant systems, causing delayed neuronal apoptosis and necrosis [16, 17]. The previous studies reported that SCI could induce mitochondrial morphological changes, oxidative damage, and apoptosis, which may correlate with the pathological mechanisms of secondary damage following SCI [18, 19]. Recently, studies report that the role of mitochondria extends beyond energy production to affect both neural homeostasis and neurodegenerative processes in the central nervous system (CNS) [19, 20]. A potentially effective therapeutic strategy for SCI is to restore mitochondria function in the injured spinal cord, improving neuron apoptosis and functional recovery.

Recently, transfer of mitochondria is emerging as a new therapy to the injured cells by decreasing ROS production, increasing ATP production and calcium buffering capacity [21]. Injured neurons are able to capture functional mitochondria from astrocytes and promote survival and plasticity [22]. Importantly, stem cells are recognized as unexceptionable donor cells for mitochondrial transfer and numerous studies have substantiated the significance of mitochondrial transfer in stem cell therapy, especially mesenchymal stem cells [23]. Mitochondria could be transferred from mesenchymal stem cells to nearby injured cells to improve cell viability [24, 25].

Our previous studies demonstrated that BMSCs could protect injured neurons and prevent neuronal apoptosis after SCI [26, 27]. Thus, we hypothesized that transfer of mitochondria from BMSCs to the injured neurons might play an important role in the protective effects of BMSCs on SCI. In the present study, we investigated the transfer of mitochondria from BMSCs to the oxygen glucose deprivation (OGD)-injured neurons. We also transplanted healthy mitochondria from BMSCs to the injured spinal cord of SCI rats to explore the protective effects of mitochondria. Furthermore, the pharmacological drugs

affecting gap junction intercellular communication (GJIC) were used to study the underlying mechanisms involved in mitochondria transfer between BMSCs and the injured neurons. Based on our findings, we provide the first evidence that transplanted BMSCs could prevent neuronal apoptosis and facilitate locomotor functional recovery via transfer mitochondria to the injured neurons after SCI.

Materials and Methods

Primary BMSCs culture and characterization

The experimental procedures were approved by the Animal Ethics Committee of Zhejiang University and were carried out in accordance with National Institutes of Health guidelines. All efforts were made to minimize the number of animals used and their suffering. BMSCs were isolated from 3 to 4 week old Sprague-Dawley male rats according to our previous study [4, 26]. BMSCs were cultured in Dulbecco's modified Eagle's medium (DMEM) with 10% fetal bovine serum (FBS, Gibco, USA) and 1% penicillin and streptomycin (Gibco, USA). Consistent to our previous study, the fluorescence-activated cell sorting (FACS) analysis revealed that BMSCs at passages 3~5 were negative for CD34 (hematopoietic marker), but expressed BMSCs lineage markers, including CD44, CD90, and CD105[27]. BMSCs were digested and washed twice with phosphate-buffered saline (PBS) to a concentration of 10^7 cells/100 μ l.

Primary cortical neuron culture

Primary cortical neuron cultures were obtained from E-18 Sprague-Dawley rat embryos. Briefly, cortices were dissected by sterile scissors in cold D-Hanks medium and then incubated in 0.25% trypsin-EDTA (ethylenediaminetetraacetic acid) for 15 min at 37°C and then terminated by 10% FBS DMEM medium. Then, the cortices were gently digested. The supernatant was collected for centrifuging at the speed of 1000 rpm/min at 4°C for 5 min and the deposit was neuron. Neurons were spread on plates coated with 25 μ g/ml poly-D-lysine (PDL, Beyotime Institute of Biotechnology, Nantong, Jiangsu, China) and cultured in 2% B27 Neurobasal medium (Gibco, Invitrogen), 1% penicillin/streptomycin and 2 mM L-glutamine (Sigma). We changed half of the medium every two days.

MitoTracker Red staining and carboxyfluorescein succinimidyl ester(CFSE)-fluorescent label

MitoTracker Red CMXRos (Molecular Probes, M7512, Invitrogen, USA) was used to visualize the mitochondria of BMSCs. BMSCs were stained with 200 nM MitoTracker Red for 20 min at 37°C. Cells

were washed twice with PBS to ensure that the excess of the dye was washed out. BMSCs were then detached and seeded for the following steps.

VSC4.1 motor neurons were pre-stained with 10 μ M carboxyfluorescein succinimidyl ester (CFSE, #C1031, green colour, Beyotime Institute of Biotechnology, Nantong, Jiangsu, China). Briefly, VSC4.1 motor neurons were seeded in 6-well plates and stained by 10 μ M CFSE (0.5 ml/well) for 30 min and washed by PBS twice. Pre-stained BMSCs and VSC4.1 motor neurons were grown in motor neuron medium, supplemented with 100U/ml penicillin and streptomycin. 4',6-diamidino-2-phenylindole (DAPI, #C1002, Beyotime Institute of Biotechnology, Nantong, Jiangsu, China) was stained for all cell nucleus after cells were fixed by paraformaldehyde.

Oxygen–Glucose Deprivation (OGD) model of VSC4.1 motor neurons

The ventral spinal cord 4.1 (VSC4.1) motor-neuron cells were cultured at 37°C with 5% CO₂ in a fully humidified incubator in RPMI1640 media containing 10% (v/v) fetal bovine serum and 1% penicillin and streptomycin. To mimic ischaemic injury of the spinal cord *in vivo*, OGD and re-oxygenation models were made to induce the death and apoptosis of VSC4.1 motor neurons and the model had slight modifications from the previous one[28]. VSC4.1 motor neurons were washed with PBS and then incubated in D-Hanks' balanced salt solution without glucose in a sealed hypoxic GENbag fitted with a catalyst (BioMérieux, Marcy l'Étoile, France) to scavenge free oxygen for 8 h. As for the non-OGD control group, cells were cultured in Hanks' balanced salt solution with a normal concentration of glucose. At the ending of time point of OGD, the OGD medium was replaced with normal medium and the cells were cultured in a chamber set at normal parameter (re-oxygenation, 37°C, 5% CO₂) for 24 h.

Co-culture of post-OGD neurons with BMSCs

Co-cultures of BMSCs and VSC4.1 motor neurons or primary cortical neurons were carried out in 6-well plates with 1 \times 10⁶ cells/well (BMSC: neurons in a 1:1 ratio) for 24 h. The transwell system was also performed in a 6-well plate (8 μ m pore). After co-culturing for 24 h, cells were fixed with 4% PFA for 15 min at room temperature and cell nuclei were stained with DAPI. The fluorescence of cell was captured using a confocal laser-scanning microscope (FluoView FV3000, Olympus Corporation, Tokyo, Japan).

Preparation of conditioned medium of BMSCs (BMSCs-CM)

In brief, BMSCs were plated at 5 \times 10⁴ cells/well and incubated in 10% FBS DMEM. The attached cells were washed three times with PBS and the medium was replaced with high glucose DMEM without serum to generate BMSCs-CM. The medium was collected after 24 h of culture and used as BMSC-CM. At the same time, mitochondria deleted medium BMSC-CM (Md-BMSC-CM) was filtered through a 0.22 μ m syringe filter which could prevent mitochondria from entering the medium and thus Md-BMSCs-CM was obtained.

Isolation of Mitochondria from BMSCs

Mitochondria were isolated from cultured BMSCs using a Mitochondria Isolation Kit (#89874, Mitochondria Isolation Kit for mammalian cells, Thermo Fisher, USA) as previously reported [29]. The Mitochondria Isolation Kit contained mitochondria isolation reagents A, B and C. Briefly, BMSCs were digested by centrifuging harvested cell suspension in a 2.0 mL microcentrifuge tube at 850 \times g for 2 min and removing the supernatant. Mitochondria Isolation Reagent A was added to BMSCs in a tube on ice. The tube was vortexed at medium speed for 5 s and incubated on ice for 2 min. Then, mitochondria isolation reagent B was added and the tube was kept on ice for 5 min, vortexing at maximum speed every minute for 5 times. Mitochondria isolation reagent C was then added, and the tube was inverted several times to mix and centrifuged at 700 \times g for 10 min at 4°C. The supernatant was transferred to a new tube and mitochondria were harvested after centrifuging at 12000 \times g for 15 min. The freshly isolated mitochondria were labelled with MitoTracker Red staining and were used in the following study.

Fluorescence microscope observation on internalization of isolated mitochondria from BMSCs in neurons

To explore whether different concentrations of mitochondria would have different efficiencies of internalization, VSC 4.1 motor neurons were pre-stained with CFSE (green colour) to visualize cell cytoplasm of neurons and then were co-cultured with two concentrations of mitochondria from BMSCs. MitoTracker Red staining enabled fluorescent measurement of internalization mitochondria based on the increase in red fluorescence as the mitochondria were internalized within the motor neurons. Then, 1 \times 10⁵ /well post-OGD VSC4.1 motor neurons were co-incubated with high concentration mitochondria (from 3 \times 10⁷ BMSCs/well) in 35 -mm glass bottom culture dishes. Next, different time periods (4 h or 24 h) were

designed to explore whether the internalization of low concentration of mitochondria was time dependent. 1×10^5 /well post-OGD VSC4.1 motor neurons in a 3.5-cm dish were co-incubated with mitochondria isolated from 1.0×10^6 /well BMSCs for 4 h or 24 h.

Mitochondria internalization in post-OGD motor neurons (OGD treatment) and in normal motor neurons (Non-OGD treatment) were both observed to confirm whether the OGD injured motor neurons would have a higher uptake rate.

The fluorescence of motor neurons was monitored using a real-time fluorescence microscope (FluoView, FV1000, Olympus, Japan). The fluorescence of cell images was captured, and the number of mitochondria internalized motor neurons was calculated by Image-J software.

FACS analysis on apoptosis rate of VSC4.1 motor neurons

VSC4.1 motor neurons (5×10^5 /well) were exposed to OGD for 8 h and cultured with isolated mitochondria (from 1.5×10^6 BMSCs/well) for 24 h. An Annexin V-FITC/ propidium iodide (PI) apoptosis kit (#AP101, Multi Sciences Biotech, Hangzhou, Zhejiang, China) was used to analyze the apoptosis rate. At the end of time point, VSC4.1 motor neurons were washed with cold PBS twice and incubated with 500 μ L binding buffer. After adding 5 μ L Annexin V-FITC and 10 μ L PI, cells were analyzed by fluorescence-activated cell sorting (FACS). Annexin-V positive and PI negative cells were defined as early necrotic cells while Annexin-V negative and PI positive cells were regarded as late necrotic cells.

Extracellular flux analysis

To detect the bioenergetics profiling of post-OGD VSC4.1 motor neuron with BMSCs derived mitochondria, the XFe96 Extracellular Flux Analyzer (Seahorse Bioscience, MA, USA) was used as previously reported [30, 31]. VSC4.1 motor neurons were seeded in XFe96 cell culture plates coated with Cell-Tak (BD Biosciences, San Jose, CA) at 1×10^4 cells/well. Some VSC 4.1 motor neurons were pretreated with 18β - glycyrrhetic acid (18β -GA, 50 μ M) or retinoid acid (RA, 10 μ M) for 8 h. Then, freshly isolated mitochondria from BMSCs (5 μ g) were added into each well and incubated. Oxygen consumption rate (OCR) measurement was performed in XF media (non-buffered DMEM) supplemented with 11 mM glucose, 2 mM L-glutamine and 1 mM sodium pyruvate under basal conditions and in response to mitochondria inhibitors: 1.5 μ M oligomycin, 50 nM trifluoromethoxy carbonylcyanide phenylhydrazine (FCCP) or 1 μ M rotenone + 5 μ M antimycin A (Sigma). OCR (pMoles/min) was measured during 2 min. The

basal respiration rate was calculated as the difference between basal OCR and OCR after inhibition of mitochondrial complex I and III with rotenone and antimycin A, respectively. The maximum respiration rate was measured following addition of the uncoupler FCCP (uncoupled rate), indicative of the maximum activity of electron transport and substrate oxidation achievable by the cells. OCR, basal oxygen consumption and maximal oxygen consumption were calculated from the primary data. Data set was analyzed by XFe-96 software and GraphPad Prism software, using one-way analysis of variance (ANOVA) calculations.

Intracellular ATP Measurement, lactate dehydrogenase (LDH) release assays and CCK-8 assay

ATP content was determined by using the ATP Assay Kit (#S0027, Beyotime Institute of Biotechnology, Nantong, Jiangsu, China) according to a previous study [32]. Briefly, two groups of VSC4.1 motor neurons (1×10^4 /well) co-cultured with mitochondria (from 3×10^4 BMSCs/well) for 24 h were washed with PBS and lysed in 100 μ L lysis buffer on ice and lysate was collected and centrifuged at $12,000 \times g$ for 3 min. In a 96-well opaque plate, 20 μ L of each supernatant was added into the wells containing 100 μ L ATP detection working dilution. The luminescence was detected by a microplate reader (SynergyMx M5, Molecular Devices, USA).

As for LDH (#C0016, Beyotime Institute of Biotechnology, Nantong, Jiangsu, China) assay, VSC4.1 motor neurons were cultured and performed as described above in the ATP assay. Culture supernatants were collected to detect the level of LDH release as measured using the CytoTox96® Non-Radioactive Cytotoxicity Assay (Nanjing Jiancheng Bioengineering Institute, Nanjing, Jiangsu, China) according to the manufacturer's instructions [33]. Experiments were performed at least in triplicate. Data were expressed as percentages of control values.

For CCK-8 (#C0041, Beyotime Institute of Biotechnology, Nantong, Jiangsu, China) assay, VSC4.1 motor neurons (1×10^4 cells/well) were seeded into 96-well plates after digestion with trypsin and five parallel wells were used for each treatment. The survival of post-OGD VSC4.1 motor neurons was assayed using a CCK-8 Kit (#C0037, Beyotime Institute of Biotechnology, Nantong, Jiangsu, China) as previously described [34]. After incubating for 2 h, cell viability was calculated by TECAN infinite M5 (Molecular Devices, USA) at the wavelength of 450 nm.

Measurement of mitochondria membrane potential

A JC-1 kit (#C2005, Beyotime Institute of Biotechnology, Nantong, Jiangsu, China) was used to assess mitochondria membrane potential [35]. VSC4.1 motor neurons were incubated with JC-1 for 20 min. Then mitochondria membrane potential was analyzed by fluorescent reader and the fluorescence intensity ratio represented the transfer of intensity on membrane potential.

Western blot analysis

For the determination of expression level of protein related to mitochondrial apoptosis and endoplasmic reticulum stress, 1×10^6 /well VSC4.1 motor neurons in 6-cm plates were co-incubated with mitochondria (mitochondria from 3×10^6 BMSCs/well) for 24 h. The following primary antibodies were used: Bcl-2 (#3498, 1:1000, Cell Signaling Technology, USA), Bak (#12105, 1:1000, Cell Signaling Technology, USA), GRP78 (#ER40402, 1:1000, HuaAn Biotechnology Co., Ltd, China), CHOP (GADD 153 Antibody (F-168): sc-575, 1:500, Santa Cruz Biotechnology, USA), P-AKT (#4060, 1:1000, Cell Signaling Technology, USA), and GAPDH (1:5000; Sigma-Aldrich, USA). After washing with T-BST, blots were incubated with infrared-labelled secondary antibody (Li-COR biosciences) for 60 min and then washed by T-BST for 3 times every 10 min. Quantification of band intensity was performed using NIH Image J software after being normalized.

To explore whether VSC4.1 and BMSCs express connexin43 and connexin32 (gap junction protein), VSC4.1 and BMSCs were harvested. Primary antibody of connexin43 (#sc-6560, 1:500, Santa Cruz Biotechnology, USA) and connexin32 (#sc-7258, 1:500, Santa Cruz Biotechnology, USA) were used.

To explore the neurite outgrowth and re-myelination in the spinal cord, the spinal cord samples at six weeks after SCI (n=3/group) were analyzed by western blot analysis. Primary antibody of GAP43 (#8945s, 1:1000, Cell Signaling Technology, USA) and myelin basic protein (MBP, #D8X4Q, 1:1000, Cell Signaling Technology, USA) were used.

FACS analysis on the exchange of endocytic organelles and mitochondria between BMSCs and neurons

FACS analysis (BD, LSR Fortessa, USA) was used to detect the exchange of endocytic organelles (including mitochondria) between BMSCs and post-OGD VSC4.1 motor neurons. BMSCs were pre-stained with MitoTracker Red CMXRos (red). VSC4.1 motor neurons were labelled with CFSE (green). In order to explore whether GJIC mediated

the exchange of mitochondria between BMSCs and neurons, the pharmacological drugs of GJIC were used and dissolved in DMSO as stocking solution. For potentiation, BMSCs were pre-incubated with gap junction potentiator RA ($10 \mu\text{M}$) for 8 h prior to co-culture. For inhibition, BMSCs were pre-incubated with gap junction inhibitor $18\beta\text{-GA}$ ($50 \mu\text{M}$) for 8 h prior to co-culture. 1×10^5 BMSCs were then digested and seeded to a 6-well plate to co-culture with post-OGD VSC4.1 motor neurons (OGD 8 h, 5×10^5 /well) for 24 h in a direct co-culture model with or without drugs. The population of red and green double labelled cells was examined by FACS analysis and was calculated by counting both red fluorescence positive and green fluorescence positive cells. The exchange rate of mitochondria from BMSCs to VSC4.1 motor neurons was calculated by counting the population of red fluorescence positive VSC4.1 motor neurons from the data of the FACS analysis.

SCI model

Sixty-three Sprague-Dawley male rats (200-220 g) were divided into 4 groups randomly (Sham group, SCI group, BMSCs treatment group and mitochondria treatment group, see supplement Figure S3). The SCI model was Allen's method as described in our previous study [27]. Rats were anaesthetized by pentobarbital (40 mg/kg , i.p). Then, the vertebral columns of the rats were exposed and a laminectomy was carried out at T10 level. A weight of 10 g from (#WH160162, Convergence Technology Co., Ltd, Shenzhen, China) was dropped from a height of 50 mm on the exposed spinal cord and the impounder was left for 20 s before being withdrawn to produce a moderate contusion in SCI group in accordance with our previous study. Immediately after SCI, both hind limbs of the rat twitched involuntarily and the tail wiggled, which meant that the injuries to the rats corresponded to the criteria of the SCI model. The sham operation animals received the same surgical procedure without the weight drop. After operation, all the rats were seamed using silk sutures 4-0 and given an injection of penicillin G (100 mg/kg , intramuscular injection) to prevent infection for 7 days and rats had easy access to food and water and their bladders were manually voided twice a day due to the paralysis until autonomic rhythm of neurogenic bladder resumed. The Basso, Beattie and Bresnahan (BBB) scale is used to evaluate the functional recovery of locomotor capacity in rats after spinal cord injury within 6 weeks. The rats were sacrificed for subsequent histological, immunohistochemistry, Masson staining, Luxol-fast-blue staining (LFB staining), western blot, TEM and immunofluorescence, respectively.

Mitochondria and BMSCs transplantation in SCI rat

Immediately after SCI, 10 μ L BMSCs (1×10^6) in BMSCs treatment rats and 10 μ L mitochondria extracted from BMSCs (3×10^6) were separately injected into the epicentre of the injured spinal cord using an electrode microneedle, while the same volume PBS were injected into Sham group and SCI + Vehicle group after operation. To confirm the localization of mitochondria in the spinal cord, three rats in the mitochondria treatment group were injected with MitoTracker-

Red pre-stained mitochondria and were sacrificed at 48 h. The lesion epicentre (4 mm) of the spinal cord was removed and prepared for cryostat sectioning.

Immunofluorescence staining

Spinal cord sections from mitochondria treatment group (n=3) with MitoTracker Red-labelled mitochondria were stained with the DAPI to visualize the nucleus. Every section was observed using the fluorescence microscope (Olympus BX61, Japan) and analyzed using Image-Pro Plus 5.0 image (Media Cybernetics Inc., Atlanta, GA, USA).

To verify that isolated mitochondria were uptaken by neurons, astrocyte or macrophage, spinal sections were stained with neuron marker MAP2 (#4542, 1:200, Cell Signaling Technology, USA), astrocyte marker GFAP (#3655, 1:100, Cell Signaling Technology, USA), macrophage marker CD11b/c (#ab1211, 1:100, Abcam, USA) and Z-stack images were photographed by confocal microscopy (FluoView FV3000; Olympus Corporation, Tokyo, Japan). Briefly, frozen spinal cord sections were washed 3 times in PBS and blocked in blocking buffer for 60 min. Then spinal cord sections were incubated overnight with primary antibody. After washing by PBS 3 times, fluorescent secondary antibodies were added. Finally, DAPI was added and then coverslips were placed.

TdT-mediated dUTP nick end labelling (TUNEL) staining

Rats from four groups (Sham group, SCI + Vehicle group, SCI+BMSCs group, SCI+Mito group, n=3) were re-anesthetized with sodium pentobarbital (60 mg/kg, i.p.) and perfused with 4% paraformaldehyde 48 h after transplantation. The lesion epicentre (4 mm) of the spinal cord was removed and prepared for cryostat sectioning which was embedded in OCT (Sakura Finetech, Tokyo, Japan). All specimens were cut into 20 μ m thick sections using a Cryostat microtome (Leica, Germany). The severity of damaged cells was detected by the one step TUNEL apoptosis assay kit (Beyotime Institute of Biotechnology, NanTong, JiangSu, China) according to our

previous method [36]. Apoptotic cells which reflected the DNA fragmentation of nuclei were TUNEL (green colour). Every section was photographed by the fluorescent microscope (FluoView FV3000; Olympus Corporation, Tokyo, Japan) and analyzed with the Image-Pro Plus 5.0 image.

Immunohistochemistry, haematoxylin and eosin (H&E), LFB and Masson staining

Six weeks after treatment, twenty-four rats (n=6/group) were chosen randomly, anesthetized, and intracardially perfused with 50 ml 0.9% NaCl, followed by 150 mL of 4% paraformaldehyde solution. The T9-T12 spinal cord segments centered on and enclosing the injured site were collected and post-fixed in 4% paraformaldehyde at 4°C overnight. Then, the spinal cords were embedded in paraffin for serial longitudinal sectioning (n=3/group) and serial transverse sectioning (n=3/group).

Longitudinal sections of spinal cord were stained with H&E staining and were observed by the light microscope (Olympus B61, Tokyo, Japan).

LFB staining was performed to visualize the myelin in spinal cord. Briefly, the longitudinal sections were immersed in alcohol (95%) for 5 minutes and LFB (0.1%) at 65°C overnight. The sections were displaced into aqueous lithium carbonate (0.05%) and rinsed several times with alcohol (70%) and then in double-distilled water, after washing in alcohol (95%) again. Finally, the slices were counterstained with cresy violet (0.1%) and were hyalinized with xylene and mounted with neutral balsam. The LFB-positive area of white matter was analyzed by Image-Pro Plus 5.0 software.

For Masson staining, the longitudinal sections were mordanted in potassium dichromate (10%) and trichloroacetic acid (10%) for 30 min, nuclei were stained with hematoxylin for 20 min, then were differentiated with hydrochloric acid and ethanol for 15 s, returned to blue with weak ammonia for 15 s, and stained with Masson solution (Cell Signaling Technology, USA) for 1 min. After rinsing with acetic acid (1%), the sections were dehydrated with ethanol, deleted with xylene I and II for 10 min to render these sections transparent and then were sealed in resin. Then the sections were photographed using a light microscope (Olympus B61, Tokyo, Japan) to observe collagen deposition.

For immunohistochemistry staining, transverse sections were incubated overnight at 4°C with GFAP antibody (GA5, #3670, 1:100, Cell Signaling Technology, USA) and neurofilament-H (NF, RMdO 20, #2836, 1:200, Cell Signaling Technology, USA) and these sections were observed by the light microscope (Olympus B61, Tokyo, Japan) and analyzed using the

Image-Pro Plus 5.0 image.

BBB score and footprint analysis

BBB scores were used to assess the severity of paralysis due to spinal cord injury according to the motor function. BBB scores were obtained by two independent examiners who were blind to four groups to evaluate at 1, 3, 5, 7, 14, 21, 28, 35 and 42 days post-surgery. Apart from BBB scores, we also performed the Footprint analysis as previous study reported [37]. Briefly, the forelimbs of rats were dipped in blue ink and the hindlimbs were stained with red ink. All rats were allowed to walk across a narrow box (7 cm in width, 80 cm in length) and the footprints of rats were observed. Stride length was measured of the distance between center pads of the ipsilateral forelimb and hind paw and the stride length was determined as the base of support.

Transmission electron microscope

In order to confirm the existence of mitochondria in BMSCs-CM, transmission electron microscope (TEM) was used. BMSCs-CM-derived mitochondria was obtained by centrifuging BMSCs-CM at the speed of 120,000 g for 30 min and then fixed with 2.5% glutaraldehyde for 4 h at 4°C, post-fixed in 1% OsO₄ (pH 7.4) and dehydrated in 70%, 90% and 100% alcohol. The sample was put in fresh Epon and then embedded in Epon overnight. Tecnai G2 Spirit120 kv microscope (FEL, Hong Kong) was used to photograph mitochondria from BMSCs-CM.

To examine the re-myelination in the spinal cord, the spinal cords sections from four groups (n=3/group) at six weeks after SCI were observed by TEM. Rats were perfused by 4% PFA and then fixed in 2.5% glutaraldehyde for 4 h and other processes were the same as the protocol described above.

Statistical analysis

Statistical analysis was analyzed by GraphPad Prism 6 software. Data was presented as mean ± SEM. Two-way ANOVA with Bonferroni post hoc test was used for BBB score and one-way analysis of variance (ANOVA) with Student's-Newman-Keuls test was used for three or more groups of the mean comparison. Unpaired student's t-test was used to analyze the mean values of two groups. Differences were considered significant at $P < 0.05$.

Results

Transfer of mitochondria from BMSCs to VSC4.1 motor neuron in direct co-culture conditions

BMSCs were pre-stained with MitoTracker Red as shown in Figure 1A. VSC4.1 motor neurons were

labelled with neuron marker MAP2 (green) as shown in Figure 1B. Primary cortical neurons were labelled with NSE marker (green) as shown in Figure 1C. Firstly, in order to explore whether intracellular materials may undergo transfer from BMSCs to VSC4.1 motor neurons or primary cortical neurons, pre-stained BMSCs (Mito Red) and neurons (CFSE) were co-cultured in a direct co-culture condition followed by confocal microscopy. Figure 1D showed that MitoTracker Red labelled mitochondria were transferred from BMSCs to neurons as evidenced by red fluorescence dots located in the body of VSC4.1 motor neurons. Secondly, we continued to determine how mitochondria were transferred and whether a tunnel was formed from BMSCs to post-OGD VSC4.1 motor neurons. Figure 1E showed that MitoTracker Red labelled mitochondria were transferred from BMSCs to post-OGD neurons through a tunneling nanotube and others may transfer through direct contact. Figure 1F showed that mitochondria were transferred from BMSCs to primary cortical neurons through a tunneling nanotube as well. We also observed the transfer of mitochondria from BMSCs to post-OGD Schwann cells in Figure S1B (see supplement figure).

Transfer of mitochondria from BMSCs to VSC4.1 motor neuron in an indirect co-culture conditions

The above results confirmed that mitochondria could be transferred from BMSCs to post-OGD neurons through direct contact or tunneling nanotubes. Meanwhile, we considered whether paracrine mechanism may also play a role in mitochondria transfer. Therefore, firstly, the post-OGD VSC4.1 motor neurons were co-cultured with BMSCs in a transwell plate (8 μm pore) for 24 h. Confocal microscopy observation showed BMSCs derived mitochondria (MitoTracker red labelled) were located inside the body of neurons (Figure 2A). Secondly, we cultured post-OGD VSC4.1 motor neurons in BMSCs-CM. Confocal microscopy observation showed MitoTracker red labelled mitochondria in the medium were internalized into the body of neurons (Figure 2B). Thirdly, after we cultured post-OGD VSC4.1 motor neurons in Md-BMSCs-CM for 24 h, confocal microscopy observation showed no MitoTracker red labelled mitochondria were in the body of neurons (Figure 2C). Fourthly, transmission electron microscope observation showed the existence of free intact mitochondria in the BMSCs-CM (Figure 2D). Moreover, FACS analysis detected the red-positive district (P4) which confirmed the free MitoTracker red labelled mitochondria in BMSCs-CM group (Figure 2E). Importantly, co-culture with

BMSCs-CM promoted the survival of post-OGD VSC4.1 motor neurons as evidenced by the increased OD value of CCK-8 (0.82 ± 0.02 vs 0.45 ± 0.03 , $p < 0.01$). However, co-culture with Md-BMSC-CM, which containing no mitochondria, had no effect on the survival of post-OGD VSC4.1 motor neurons (0.44 ± 0.02 vs 0.45 ± 0.03 , $p > 0.05$, Figure 2F).

Internalization of isolated mitochondria from BMSCs into post-OGD neurons and its effect

We have demonstrated that the transfer of mitochondria promoted the survival of post-OGD VSC4.1 motor neurons. This result suggested that transplantation of mitochondria might be a helpful treatment to rescue injured motor neurons. Then, we isolated the intact mitochondria from BMSCs and explored whether these fresh isolated mitochondria could be internalized into post-OGD motor neurons.

Firstly, we found that if the mitochondria at a higher concentration (from 3×10^7 BMSC/well, high concentration), the internalization speed was faster. Confocal microscopy observation confirmed that almost 100% of post-OGD neurons contained internalized mitochondria within 30 min (Figure 3A). Internalization of low concentration of mitochondria (from 1×10^6 BMSC/well) into injured neurons was obvious at 4 h ($41.02 \pm 0.7\%$, $p < 0.01$) and was sharply increased at 24 h ($97.79 \pm 0.7\%$, $p < 0.01$, Figure 3B). Moreover, the percentage of internalized mitochondria into the post-OGD neurons was higher than that in Non-OGD neurons (41.02 ± 0.72 vs 28.14 ± 1.14 , $p < 0.01$, Figure 3C). These data indicated that the internalization of mitochondria was dose dependent and time dependent.

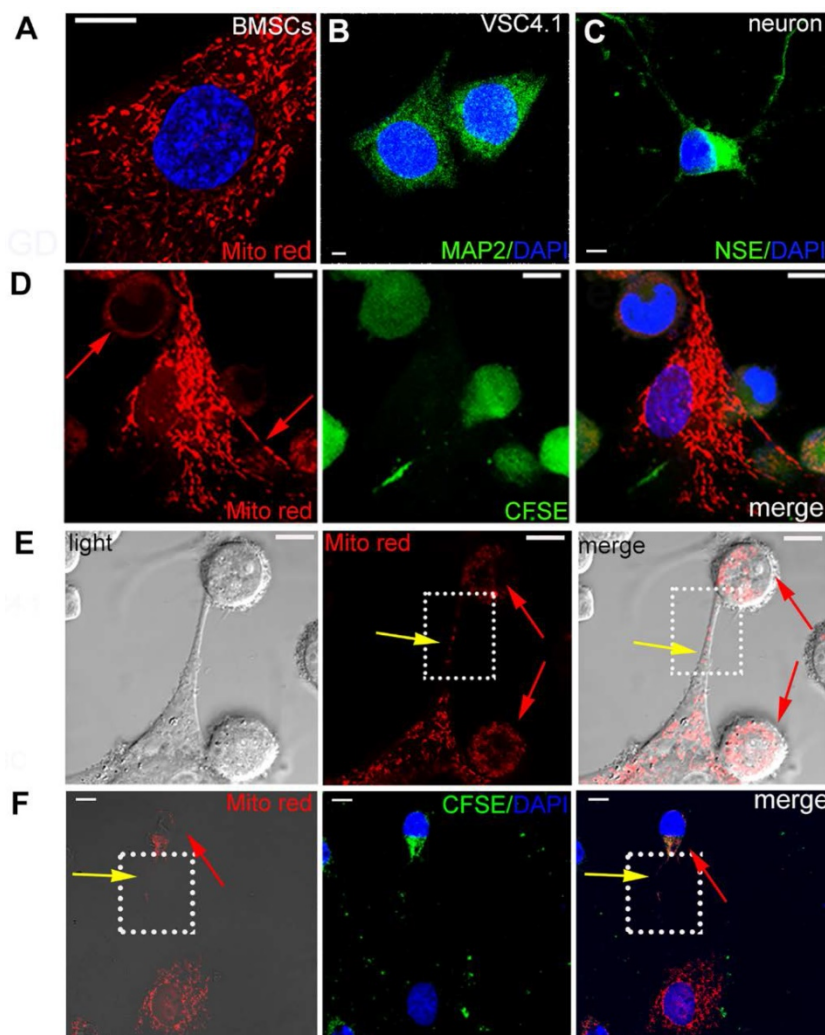


Figure 1. Transfer of mitochondria from BMSCs to VSC4.1 motor neurons in a direct co-culture condition. (A) BMSCs were stained with MitoTracker red. Nuclear staining was shown in blue (DAPI). Scale bars: 10 μ m (B) VSC4.1 motor neurons were stained with neuron marker MAP2, Scale bars: 5 μ m (C) Primary cortical neurons were stained with neuron marker NSE, Scale bars: 10 μ m (D) Mitochondria from BMSCs (MitoTracker red) transferred into pre-stained CFSE VSC4.1 motor neurons (OGD, 8 h) Scale bars: 10 μ m. (E) VSC4.1 motor neurons (OGD, 8 h) were co-cultured with BMSCs and photographed in a light scope. Mitochondria were transferred through the nanotubular-like structure to VSC4.1 motor neurons. Scale bars: 10 μ m. (F) Primary cultured cortical neurons (OGD, 4 h) were co-cultured with BMSCs. Mitochondria transfer was confirmed from BMSCs to injured neurons, Scale bars: 10 μ m

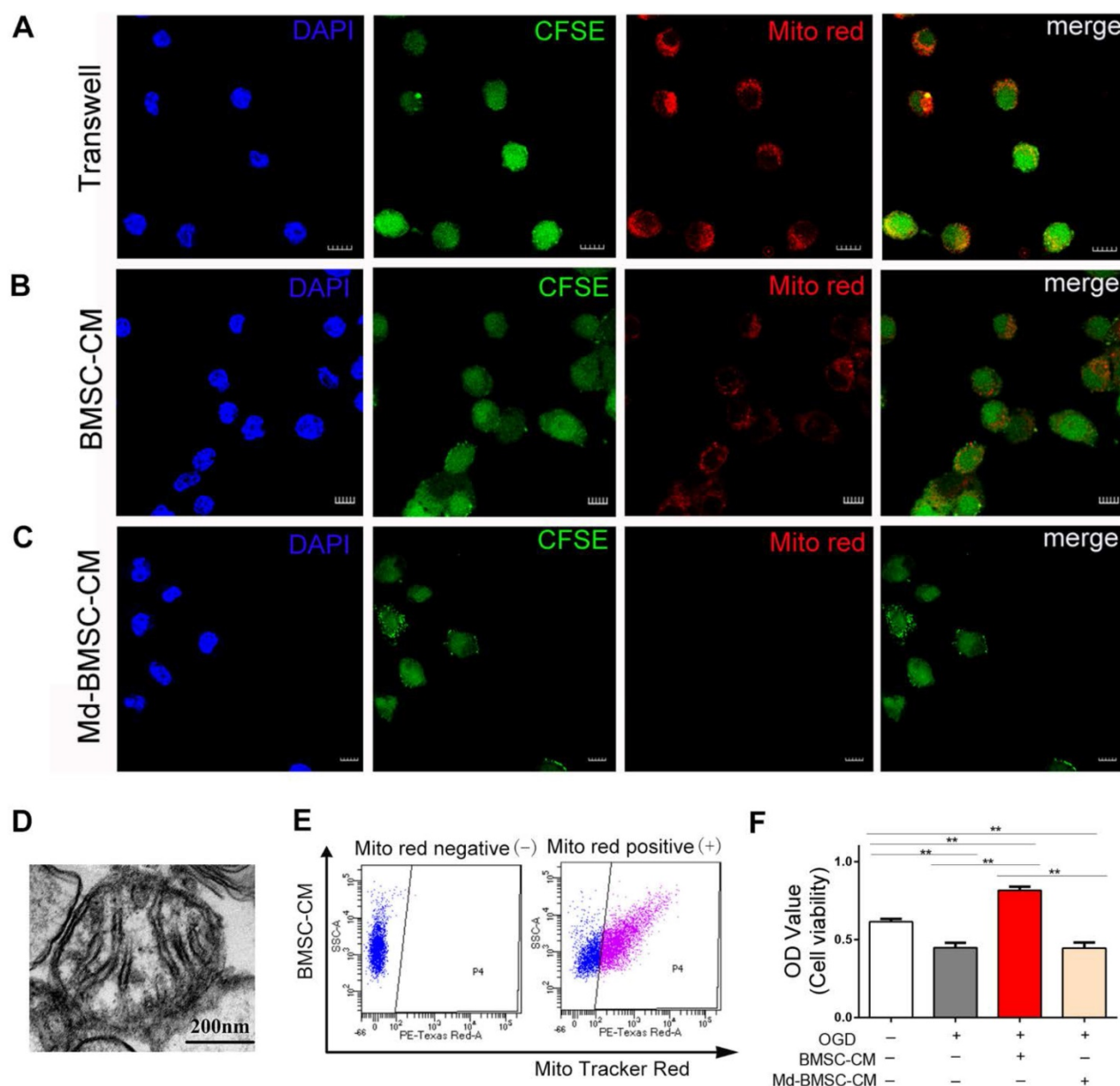


Figure 2. Transfer of mitochondria from BMSCs to VSC4.1 motor neurons in an indirect co-culture condition. (A) In a transwell system, VSC4.1 motor neurons (CFSE staining, green, OGD 8 h) were co-cultured with BMSCs (MitoTracker red) for 24 h. Mitochondria from BMSCs were transferred to VSC4.1 motor neurons. Scale bars: 10 μ m. (B) VSC4.1 motor neurons (OGD 8 h) were cultured with BMSC-CM for 24 h. Mitochondria were internalized into VSC4.1 motor neurons. Scale bars: 20 μ m. BMSC-CM = BMSCs conditioned medium. (C) VSC4.1 motor neurons (OGD 8 h) were cultured with Md-BMSC-CM for 24 h, Md-BMSC-CM = Mitochondria depleted- BMSC-CM which was filtered by 0.22 μ m syringe filter. Scale bars: 10 μ m. (D) TEM analysis demonstrated that free mitochondria were detected within the conditioned medium of BMSCs (BMSC-CM), Scale bars: 200 nm. (E) FACS analysis confirmed the mitochondria particle were in BMSCs-CM but not in Md-BMSC-CM. (F) Cell viability was determined by CCK-8 assay. Data are shown as the mean \pm SEM of the ratio for light absorbance at 450 nm. ** $P < 0.01$.

ATP content was measured in injured motor neurons with or without mitochondria treatment. The content of ATP in OGD group was decreased to approximately one-third of that in control group. However, ATP content was significantly increased in the mitochondria treatment group (2.22 ± 0.09 nmol/mg protein *vs* 1.75 ± 0.08 nmol/mg protein, Figure 3D). It was interesting to find that the enhanced intracellular ATP content in neurons co-incubated with mitochondria was not much

different with that in neurons co-cultured with BMSCs (2.22 ± 0.09 *vs* 2.48 ± 0.03 , $p > 0.05$, Figure 3D). It meant that mitochondria delivery might have the same protective efficiency as BMSCs *in vitro* OGD neuron model.

In addition, mitochondrial membrane potential was measured by the sensitive fluorescent probe JC-1 kit. The red/green fluorescent ratio was higher in mitochondria group than that in OGD group (3.89 ± 0.24 *vs* 2.31 ± 0.22 , $p < 0.01$, Figure 3E).

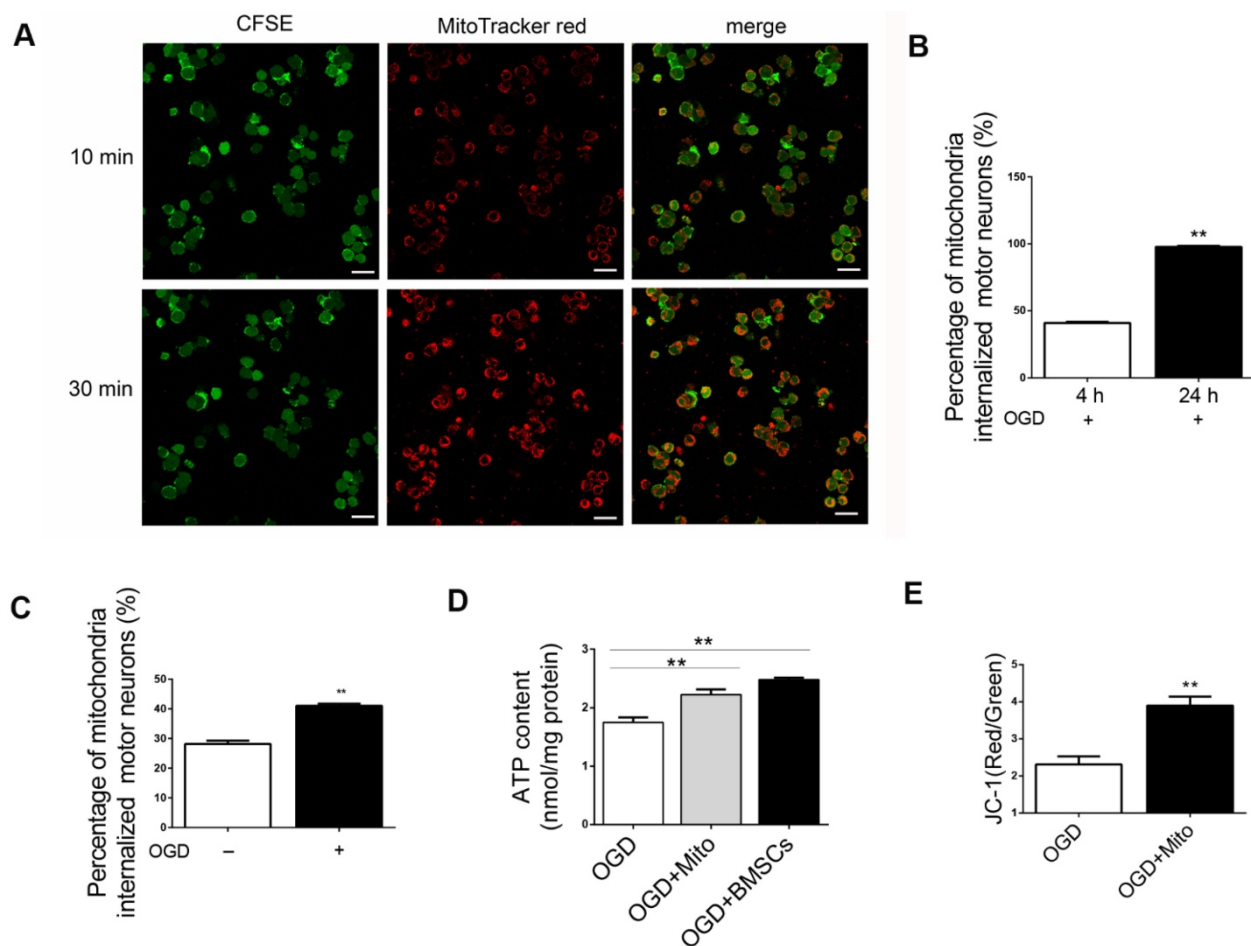


Figure 3. Internalization of isolated mitochondria from BMSCs in post-OGD VSC4.1 motor neurons and its effects on ATP and membrane potential. (A) Representative fluorescent micrographs of isolated mitochondria from BMSCs (from 3×10^7 BMSCs/well, high concentration) were co-incubated with post-OGD VSC4.1 motor neurons (1×10^5 /well) for 10 min (upper panel) and 30 min (lower panel). Scale bars:30 μ m. (B) Cell numbers of post-OGD VSC4.1 motor neurons (1×10^5 /well) with internalized mitochondria (from 1×10^6 BMSC/well, low concentration) were determined by fluorescent microscopy following 4 h and 24 h of co-incubation. The data are presented as mean \pm SEM from three independent experiments. $**P < 0.01$. (C) Cell numbers of motor neurons (normal and post-ODG) with internalized mitochondria (low concentration of mitochondria, from 1×10^6 BMSC/well) were determined by fluorescent microscopy following 4 h of co-incubation. $**P < 0.01$, vs normal neuron group. (D) VSC4.1 motor neurons (OGD, 8h) were co-incubated with mitochondria (OGD + Mito), with BMSCs (OGD+BMSCs) or Vehicle (OGD+Vehicle) for 24 h. ATP content was determined by ATP Assay Kit. The data are presented as mean \pm SEM from three independent experiments. $**P < 0.01$, vs OGD group. (E) Mitochondria membrane potential was measured by JC-1 kit. The data are presented as mean \pm SEM from three independent experiments. $**P < 0.01$, vs OGD group.

Mitochondria internalization improved the bioenergetics profile of post-OGD neurons

We also investigated the effect of mitochondria derived from BMSCs on the bioenergetics profile of post-OGD VSC4.1 motor neurons. After adding the mitochondria into the wells, post-VSC4.1 motor neurons containing mitochondria were collected for extracellular flux analysis. Compared to normal VSC4.1 motor neurons, post-OGD motor neurons showed decreased values of OCR and ECAR (Figure 4A-C). The basal respiration was decreased from 78.2 ± 2.7 pMoles/min to 36.7 ± 3.6 protein ($P < 0.01$). The maximal respiration was reduced from 69.3 ± 4.6 pMoles/min to 19.0 ± 1.2 pMoles/min ($P < 0.01$). Interestingly, BMSCs derived mitochondria significantly improved the bioenergetics profile of post-OGD VSC4.1 motor neurons. The basal respiration was

increased to 55.8 ± 4.0 pMoles/min and the maximal respiration was elevated to 37.3 ± 2.1 pMoles/min. RA significantly increased the basal respiration to 71.3 ± 4.1 pMoles/min and the maximal respiration to 56.7 ± 1.6 pMoles/min, while 18β -GA significantly decreased the basal respiration to 62.5 ± 2.7 pMoles/min and the maximal respiration to 32.0 ± 1.7 pMoles/min ($P < 0.01$, Fig. 4D-E).

Mitochondria internalization decreased OGD-induced apoptosis, promoted survival of neurons and altered the expression of apoptosis related proteins in post-OGD VSC4.1 motor neurons

LDH leakage assay showed that the release of LDH was significantly decreased in the mitochondria treatment group as compared with that in the OGD

group (63.40 ± 0.05 fold of OGD, $P < 0.01$, Figure 4F). FACS analysis showed the total apoptotic number was increased in OGD group (2.50 ± 0.17 fold of control), which was decreased by mitochondria treatment (1.49 ± 0.09 fold of control, $P < 0.01$, Figure 5A). The early apoptosis rate was significantly decreased by mitochondria treatment (4.70 ± 0.22 fold of control), which may suggest that the protection mainly affect the early stage of apoptosis (Figure 5B).

The expressions of apoptosis-related proteins were examined by western blotting assay (Figure 5C). As compared to the control group, the ration of Bcl₂/Bak in the OGD group was decreased. The ration of Bcl₂/Bak was increased in the mitochondria group compared to OGD group (0.28 ± 0.01 fold of control *vs* 0.52 ± 0.05 fold of control, $P < 0.01$, Figure 5D). The expression levels of Grp78 and Chop protein were significantly higher in the OGD group, which were slightly decreased in the mitochondria group (2.16 ± 0.10 fold of control *vs* 1.42 ± 0.13 fold of control, 8.33 ± 0.75 fold of control *vs* 3.80 ± 0.65 fold of control, $P < 0.01$, Figure 5E-F). The expression level of P-Akt protein was lower in the OGD group, which was slightly increased in the mitochondria group (0.83 ± 0.01 fold of control *vs* 0.91 ± 0.02 fold of control, $P < 0.01$, Figure 5G).

Identification of co-localization of mitochondria and apoptosis after SCI

After SCI, rats were injected with MitoTracker red pre-stained mitochondria into the spinal cord and rats were sacrificed at 48 h. The red fluorescence showed that the MitoTracker red positive mitochondria were localized inside the injured parenchyma (Figure 6A). Figure 6B shows the schematic diagram of injection site. Figure 6C-D showed the mitochondria were in the body of neurons (MAP2, green), which meant neurons could uptake mitochondria *in vivo*. Figure 6E-F showed mitochondria were also in the body of astrocytes (GFAP, green) and macrophages (CD11b/c, green) but with less number of mitochondria incorporated into cells.

TUNEL staining showed that apoptotic cells were rare in sham group, whereas many apoptotic cells were in SCI group (Figure 7A-B). Treatment with BMSCs or mitochondria significantly decreased the number of apoptotic cells. The number of apoptotic cells in BMSCs group (31.0 ± 4.00) and mitochondria group (25.67 ± 5.51) were remarkably lower than that in SCI group (52 ± 6.08), but they were still higher than that in sham group (2.7 ± 1.52 , $P < 0.01$, Figure 7C).

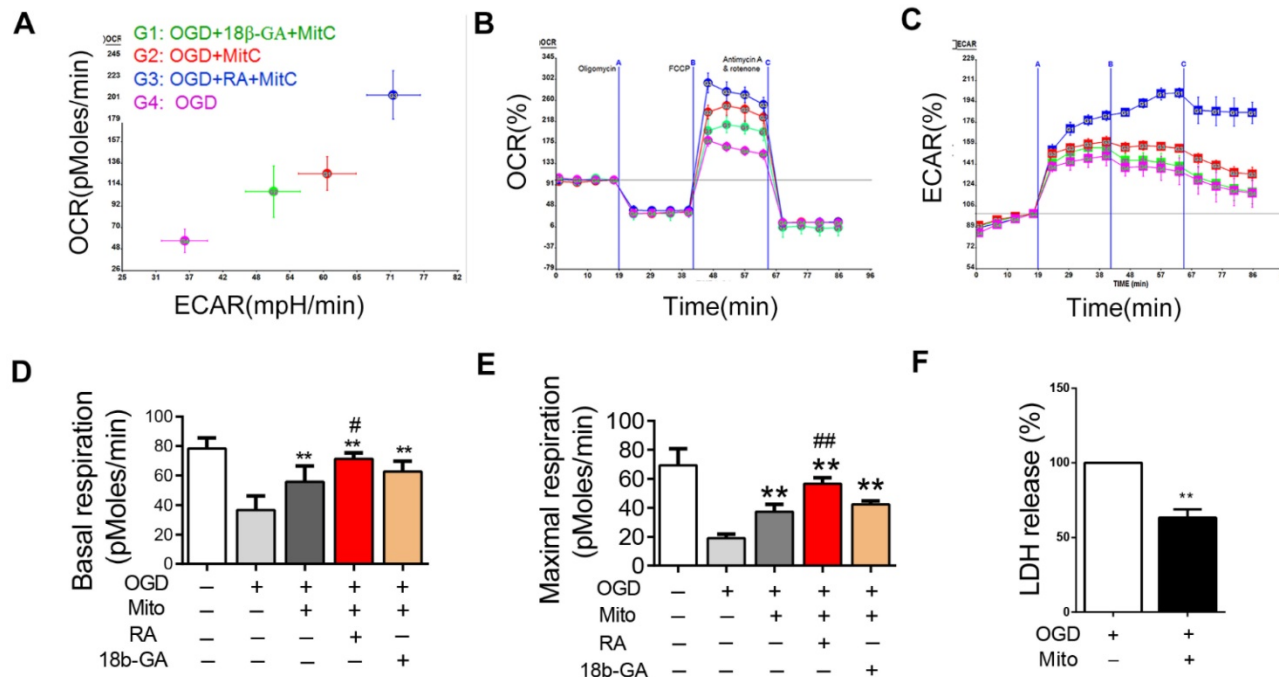


Figure 4. Mitochondria internalization improved the bioenergetics profile in post-ODG VSC4.1 motor neurons. (A-C) Representative oxygen consumption (OCR) rate curves of VSC4.1 motor neurons (OGD for 8 h) were generated by the Seahorse apparatus. OCR in post-ODG motor neurons was significantly increased by co-culture with mitochondria, which was promoted by a gap junctional intercellular communication (GJIC) potentiator retinoid acid (RA, 10 μM), but was inhibited by 18β-GA (50 μM, inhibitor). (D-E) Significant improvement in respiration (basal and maximal) was observed in the mitochondria treatment group, which was promoted by RA but inhibited by 18β-GA. Each data point is presented as mean ± SEM. ** $P < 0.01$, vs OGD group; ## $P < 0.05$, ### $P < 0.01$ vs OGD + Mito group, n=6. (F) Post-ODG VSC4.1 motor neurons were co-incubated with mitochondria (OGD + Mito group). Cell injury was determined by extracellular LDH assay. The data are expressed as percentage relative to OGD group and presented as mean ± SEM from two independent experiments, ** $P < 0.01$ vs OGD group.

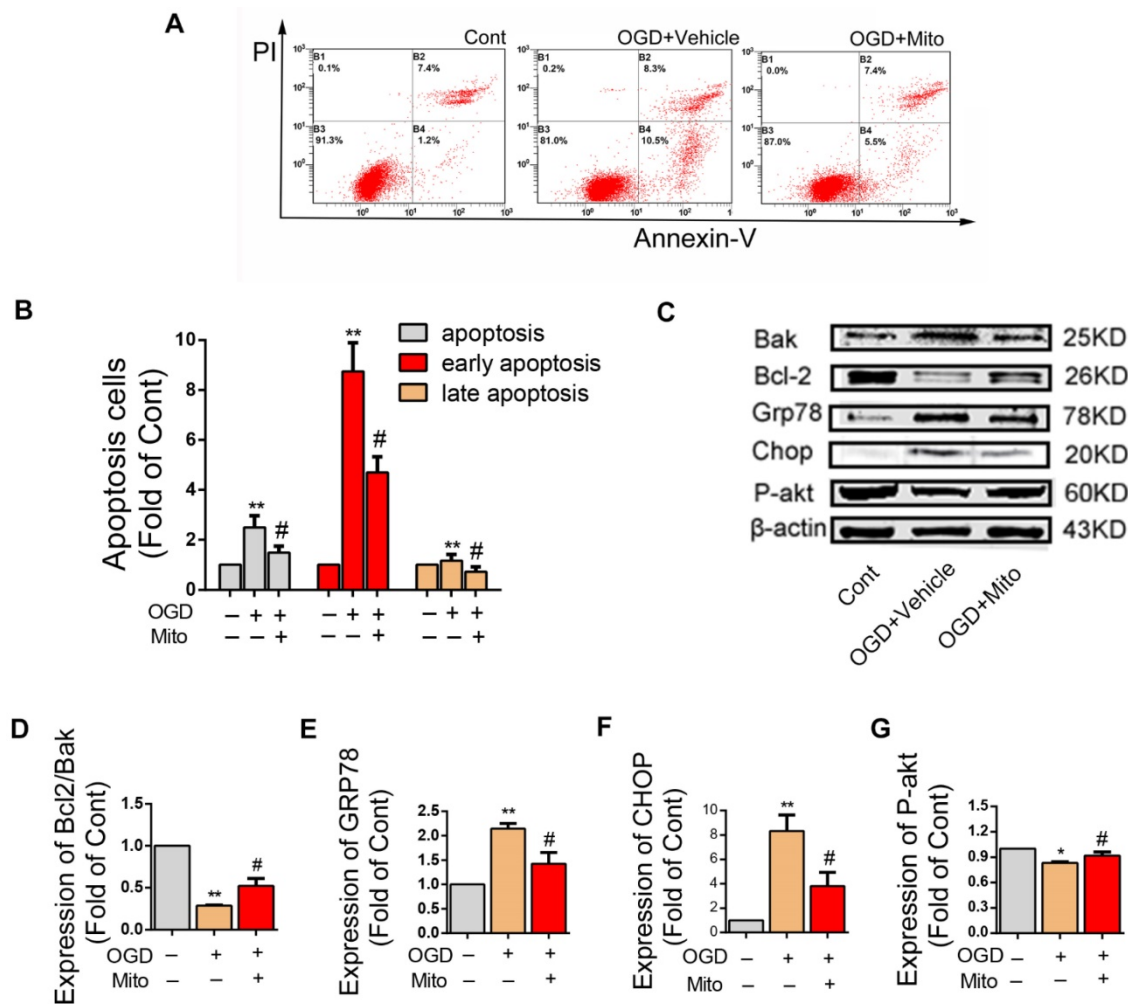


Figure 5. Mitochondria internalization altered apoptosis rate and the expression of apoptosis related proteins in post-ODG VSC4.1 motor neurons. (A-B) Post-ODG VSC4.1 motor neurons were co-incubated with mitochondria for 24 h. The apoptosis rate of neurons were analyzed by FACS analysis. Each data point is presented as mean \pm SEM. ****** $P < 0.01$, vs normal group; **#** $P < 0.05$, vs OGD group, $n=8$. (C) Expression levels of Bcl-2, Bak, GRP78, CHOP and P-AKT were analyzed by western blot assay in the Control, OGD+Vehicle and OGD+Mito groups. (D-G) Quantification of the optical densities of the protein to determine the levels of protein expressed as percentages of control values. The data are presented as mean \pm SEM from three independent experiments. ****** $P < 0.01$, vs control group; **#** $P < 0.05$ vs OGD+Vehicle group.

Mitochondria transplantation improved locomotor function recovery in SCI rats

BBB scores were significantly increased both in BMSCs and mitochondria groups as compared with SCI group. BBB score was 4.1 ± 0.40 ($P < 0.01$) at 3 weeks and 5.5 ± 0.50 ($P < 0.01$) at 6 weeks in the SCI group. The score in the mitochondria group (mitochondria from 3×10^6 BMSCs/each rat) was not significantly different relative to that in the BMSC group (1×10^6 BMSCs/each rat) at 3 weeks (7.0 ± 0.70 vs 9.8 ± 0.30 , $P > 0.05$) and at 6 weeks (9.8 ± 0.80 vs 9.3 ± 0.90 , $P > 0.05$, Figure 8A).

Footprints were evaluated at 6 weeks after SCI rats. Forelimb footprints showed in blue and the hind limb footprints showed in red (Figure 8B). The recovery of coordination could be showed in the length of stride, which meant the overlap of the forepaws and hind paws represent good

coordination. The stride length in the SCI+BMSCs group and the SCI+Mito group were significantly less than that in the SCI+Vehicle group (3.06 ± 0.23 fold of Sham, 3.80 ± 0.12 fold of Sham vs 4.50 ± 0.08 fold of sham, Figure 8C).

Mitochondria transplantation altered the expression of GAP43 and MBP and TEM

The expression levels of GAP43 (Figure 8D) were increased in the SCI+BMSCs and SCI+Mito group as compared with the SCI+Vehicle group, but they were still less than that in the Sham group (0.82 ± 0.07 fold of Sham, 0.75 ± 0.09 fold of Sham vs 0.50 ± 0.07 fold of Sham, Figure 8E). The expression level of MBP (Figure 8D) in the SCI+Vehicle group (0.44 ± 0.04 fold of Sham) was less than that in the SCI+BMSCs group (0.70 ± 0.10 fold of Sham) and the SCI+Mito group (0.78 ± 0.10 fold of Sham, Figure 8F).

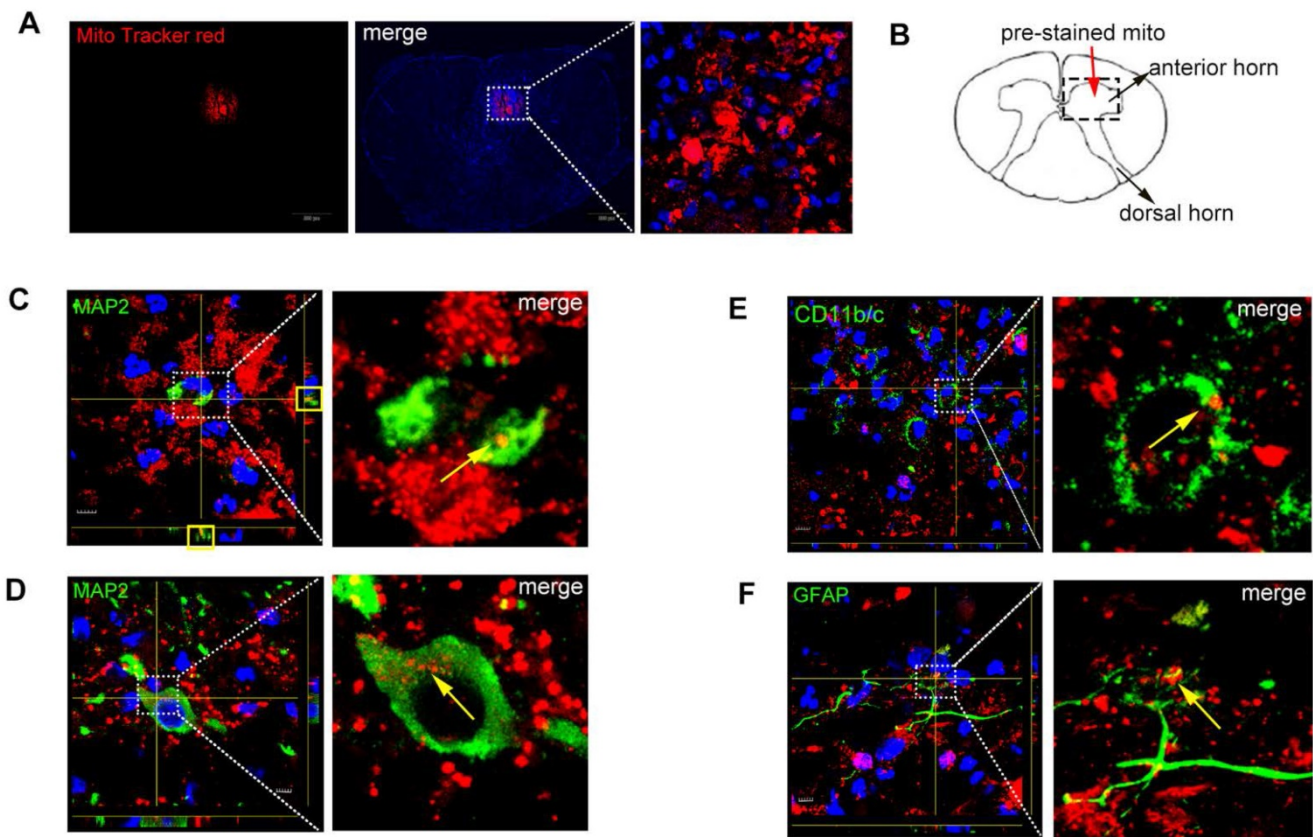


Figure 6. Co-localization of mitochondria and neurons. (A) Spinal cord injury rats with MitoTracker Red pre-stained mitochondria were injected into the spinal cord. In the injured spinal cord sections, the blue fluorescence showed that the nucleus with the DAPI, the red fluorescence showed that the MitoTracker red-positive mitochondria were localized inside the injured parenchyma. Scale bars: 50 μ m. (B) Schematic diagram of spinal cord. (C-F) Spinal cord slices were stained with MAP2, GFAP and CD11b/c. Co-localization of mitochondria (MitoTracker Red) with different cell markers in Z-stack images photographed by confocal laser scanning microscopy. GFAP: marker of astrocytes, CD11b/c: marker of macrophage; MAP2: marker of neurons, Scale bars: 5 μ m.

Transmission electron microscopy results revealed the great improvement in myelin sheath and axon integrity of the treatment groups compared to the SCI + Vehicle group (Figure 8G). Relative myelin thickness was calculated as the ratio of axon diameter to the fiber caliber (total diameter of axon plus myelin sheath). G-ratio in the SCI+BMSCs group (0.45 ± 0.04 fold of Sham) and the SCI+Mito group (0.50 ± 0.03 fold of Sham) groups were larger than that in the SCI+Vehicle group (0.20 ± 0.02 fold of Sham, Figure 8H).

Histological staining and immunohistochemistry in the injured spinal cord

H&E staining was presented in Figure 9A. Figure 9F showed the ratio of cavity area in the SCI+BMSCs group (0.75 ± 0.01 fold of SCI group, $P < 0.01$) and SCI+Mito group (0.88 ± 0.01 fold of SCI group, $P < 0.01$) were smaller than that in the SCI+Vehicle group. Meantime, LFB staining (Figure 9B) showed the area of myelin sheath in the SCI+BMSCs group (1.39 ± 0.05 fold of SCI + Vehicle group, $P < 0.01$, Figure 9G) and the SCI +Mito group

(1.37 ± 0.04 fold of SCI group, $P < 0.01$, Figure 9G) were larger than that in the SCI + Vehicle group. Masson staining showed the same trend for the area of glial scar (Figure 9C). The area of glial scar in the SCI+BMSCs group (0.55 ± 0.03 fold of SCI + Vehicle group, $P < 0.01$) and in the SCI+Mito group (0.62 ± 0.02 fold of SCI + Vehicle group, $P < 0.01$) were larger than that in the SCI + Vehicle group (Figure 9H).

Treatment with BMSCs or isolated mitochondria increased the positive area of NF (1.36 ± 0.09 fold of SCI + Vehicle group, 1.52 ± 0.05 fold of SCI + Vehicle group, $P < 0.01$, Figure 9D, Figure 9J) in the ventral horn of the spinal cord, while slightly decreased positive staining area of GFAP ($0.98 \pm 2\%$ fold of SCI + Vehicle group, $0.99 \pm 2\%$ fold of SCI + Vehicle group; $P < 0.01$, Figure 9E and Figure 9K).

GJIC-mediated the transfer of mitochondria from BMSCs to VSC4.1 motor neuron

Next, we studied the mechanisms of mitochondria transfer. Gap junctions, composed of connexin protein subunits, provide important channel for intercellular communication. Firstly, FACS analysis was performed to reveal whether GJIC played the role

in the transfer of mitochondria from BMSCs to VSC4.1 motor neuron. FACS analysis showed the population of double labelled cells was $1.2 \pm 0.8\%$ at 0 h, but significantly increased to $58.0 \pm 0.9\%$ (Figure 10A-B). The population of double-labelled cells was sharply increased by RA ($83.3 \pm 3.3\%$, $P < 0.01$, Figure 10B). The population of double-labelled cells was significantly decreased by 18β -GA ($44.3 \pm 1.1\%$, $P < 0.01$, Figure 10B). The exchange rate of mitochondria was $30.8 \pm 1.3\%$ after 24 h of co-culture, which was significantly increased to $59.2 \pm 7.3\%$ by RA, but was significantly decreased to $15.8 \pm 0.4\%$ by 18β -GA (Figure 10C). Secondly, western blot assay was conducted to confirm whether the gap junction connexins were expressed in BMSCs and neurons. Western blot assay showed that gap junction connexin43 protein was expressed in BMSCs but not in VSC4.1 motor neurons, while gap junction connexin32 was expressed in VSC4.1 motor neurons but not in BMSCs (Figure 10D), which meant they might form the heterotypic gap junction by connexin43 and connexin32 between BMSCs and neurons.

Discussion

The current study was the first to assess the potential role and underlying mechanisms involved in mitochondria transfer from BMSCs to the injured neurons after SCI. The present results demonstrated the transfer of mitochondria from BMSCs to VSC4.1 motor neurons not only through tunnelling nanotubes or direct contact, but also in a paracrine manner. Post-OGD VSC4.1 motor neurons could uptake more mitochondria from BMSCs than that of normal motor neurons. Inhibition of GJIC with 18β -glycyrrhetic acid [38] reduced mitochondria transfer, while activation of GJIC with RA [39] increased mitochondria transfer. Internalization of mitochondria increased the content of ATP, decreased LDH leakage and apoptosis in neurons. Furthermore, we transplanted BMSCs derived mitochondria to the injured spinal cord of SCI rats and found that mitochondria could decrease neuronal apoptosis and promote functional recovery. These findings proved a novel mechanism of protection of BMSCs by transfer of mitochondria to neurons via gap junction.

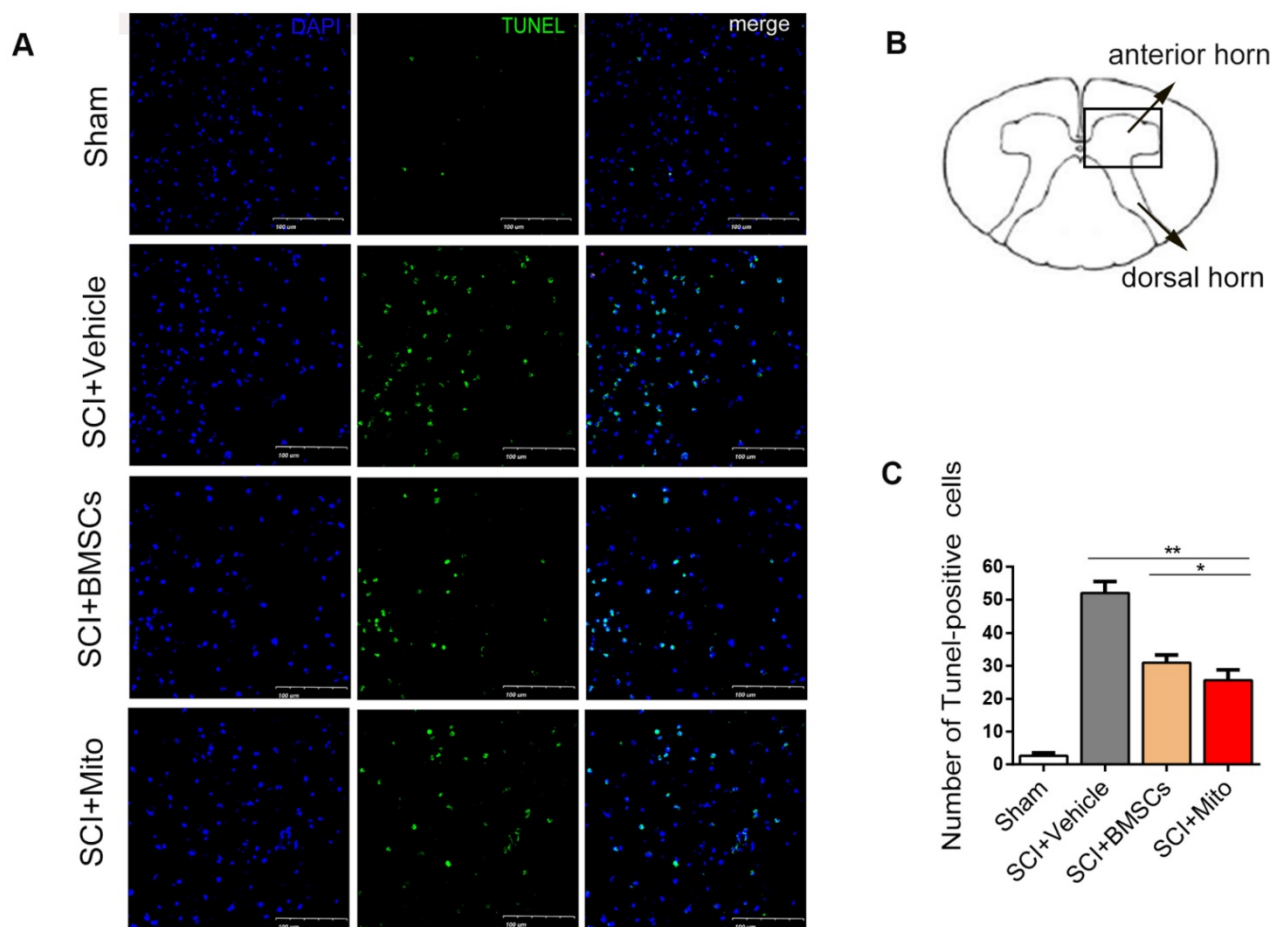


Figure 7. Mitochondria transplantation decreased apoptosis in the ventral horn of spinal cord after SCI. TUNEL staining was used to observe the apoptosis of the cells. (A) TUNEL positive cells were stained with green. Scale bars: 100 μ m. (B) Schematic diagram of spinal cord. (C) Statistics of the number of TUNEL staining positive cells. Data are presented as mean \pm SEM. * $P < 0.05$, ** $P < 0.01$, $n = 3$.

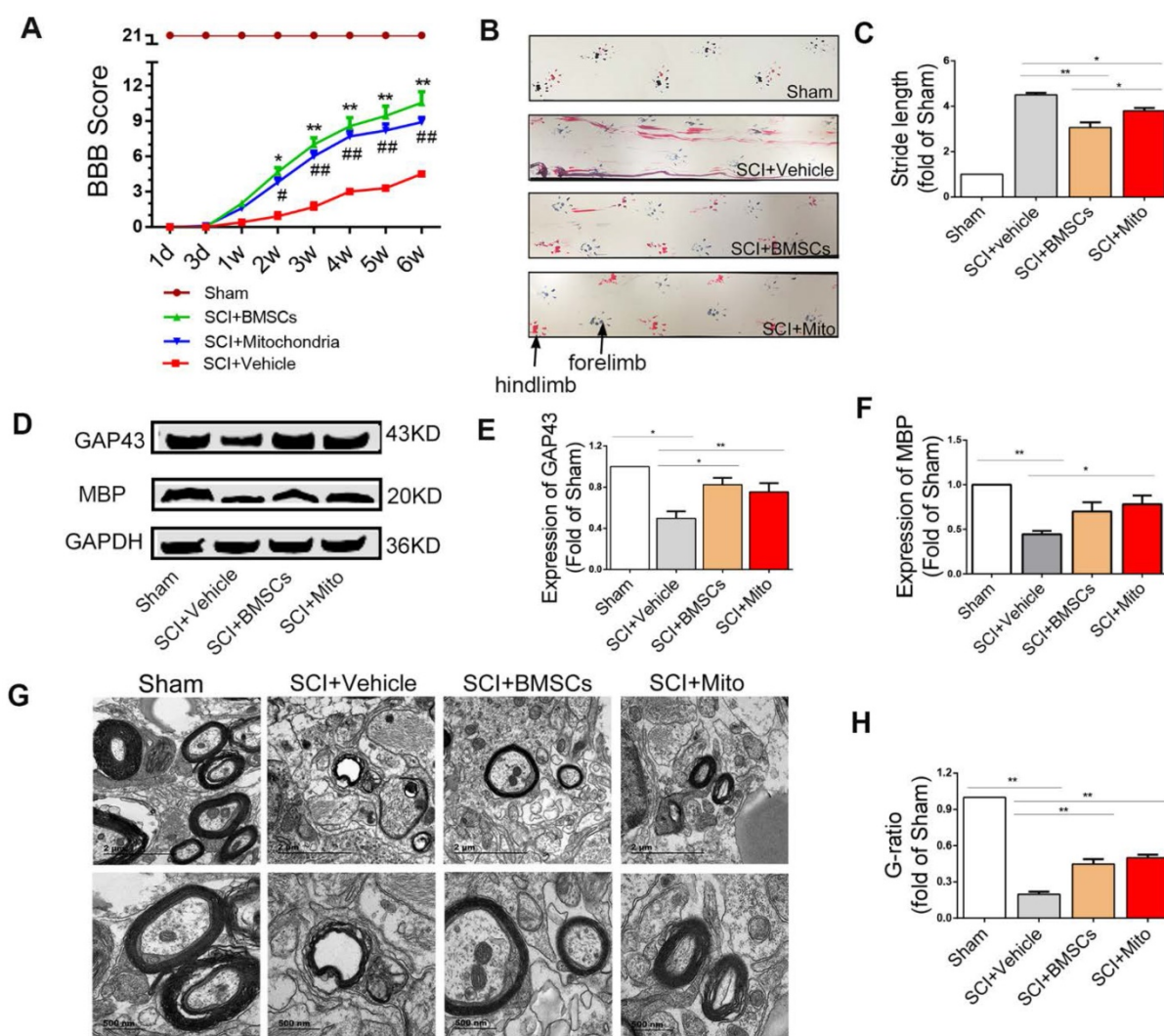


Figure 8. Mitochondria transplantation improved locomotor function recovery at 6-week after SCI. (A) BBB scores were significantly increased in both BMSCs and mitochondria treatment groups compared to the SCI+Vehicle group within 6 weeks after transplantation. * $P < 0.05$, ** $P < 0.01$, ### $P < 0.01$ vs SCI + Vehicle group. (B) Photos of rat footprints at 6-week rats. The forelimb footprints showed in blue and the hindlimb footprints showed in red. (C) Stride length was used to evaluate the coordination of locomotion. The distances in treatment groups were less than that in the SCI+Vehicle group, which showed better base of support. The data were expressed as fold of Sham and presented as mean \pm SEM. (D) Expression levels of protein of GAP43 and MBP were analyzed by western blot assay in the Sham, SCI + Vehicle, SCI + BMSCs and SCI + Mito groups. (E-F) The data were expressed as the fold of Sham and presented as mean \pm SEM from three independent experiments. (G) TEM was performed to observe the regeneration of myelin sheath. Lower panel pictures were higher magnification of myelin sheath. Scale bar in upper panel: 2 μ m. Scale bar in lower panel: 500 nm. (H) Quantification of g-ratio of axons was analyzed by IPP, each data was presented as mean \pm SEM, $n = 6$, * $P < 0.05$, ** $P < 0.01$.

The secondary SCI could be initiated several minutes after SCI and last for several weeks or months [40]. It induced progressive axon demyelination, microglia activation, mitochondrial dysfunction, and neuronal cell apoptosis [41-43]. As an important organelle providing majority energy in eukaryotic cells, mitochondria are disrupted after SCI [16, 44]. Stringent and efficient ATP is needed to maintain electrical homeostasis and accommodating neurotransmitters in neurons. Mitochondria dysfunction can cause loss of ATP and inactivation of ATP-dependent ion pumps. This dysfunction ultimately leads to excitotoxicity, calcium overload and eventual pathology in the central nervous system [45, 46], revealing that restoring the function of

mitochondria or replacement of damaged mitochondrial could improve neuronal bioenergetics profile. The present results demonstrated that mitochondria could significantly improve the bioenergetics profile of post-OGD VSC4.1 motor neurons. The basal respiration and the maximal respiration were both elevated. Furthermore, mitochondria internalization decreased OGD-induced apoptosis and promoted neurons survival. It is important to find that injured motor neurons are capable of capturing healthy mitochondria from BMSCs to produce ATP, reduce apoptosis, and improved bioenergetics profile. These results help us to understand that mitochondria transfer might be the protective mechanism involved in transplantation of BMSCs in SCI rats. At the same

time, we measured the ATP content and OD Value of BMSCs which were sorted by FACS after co-culture with post-OGD VSC4.1 neuron motors (Figure S2A). The ATP content and CCK-8 assay of BMSCs (after sorting) showed no difference from normal BMSCs (Figure S2B-C).

Moreover, we transplanted MitoTracker Red labelled mitochondria or BMSCs to the injured spinal cord of SCI rats. We confirmed that transplanted mitochondria were internalized by neurons *in vivo*, less was internalized by astrocytes or macrophages. Mitochondria transplantation decreased the number of apoptotic cells in the early stage of SCI and reduced the area of lesion cavity, glial scar, and the number of GFAP positive cells in the late stage of SCI. Meanwhile, mitochondria transplantation increased the area of myelin sheath and the number of NF positive cells, the expression level of GAP43 and promoted myelin regeneration. The most important finding was that mitochondria or BMSCs treatment both improved BBB score and footprint behavior at 3

and 6 weeks after transplantation.

Previous studies have reported the existence of nanotubular structures mediating the transfer of organelles from other cells [47, 48]. Nanotubular structures can transfer many organelles, as small molecules or ions, or mitochondria, lysosomes, and endosomal vesicles [49, 50]. Connexin oligomerization forms gap junctions that regulate intercellular mitochondrial transfer by formation of nanotubes [51, 52]. Mitochondria acquisition by the alveolar cells through gap junctions triggered the restoration of ATP levels and increased the secretion of pulmonary surfactant [24]. In present study, FACS analysis revealed that GJIC played a role in the transfer of mitochondria from BMSCs to VSC4.1 motor neuron. GJIC potentiator RA or inhibitor 18 β -GA could regulate the exchange of mitochondria. In addition, western blot assay revealed that they might form the heterotypic gap junction by connexin43 and connexin32 between BMSCs and neurons.

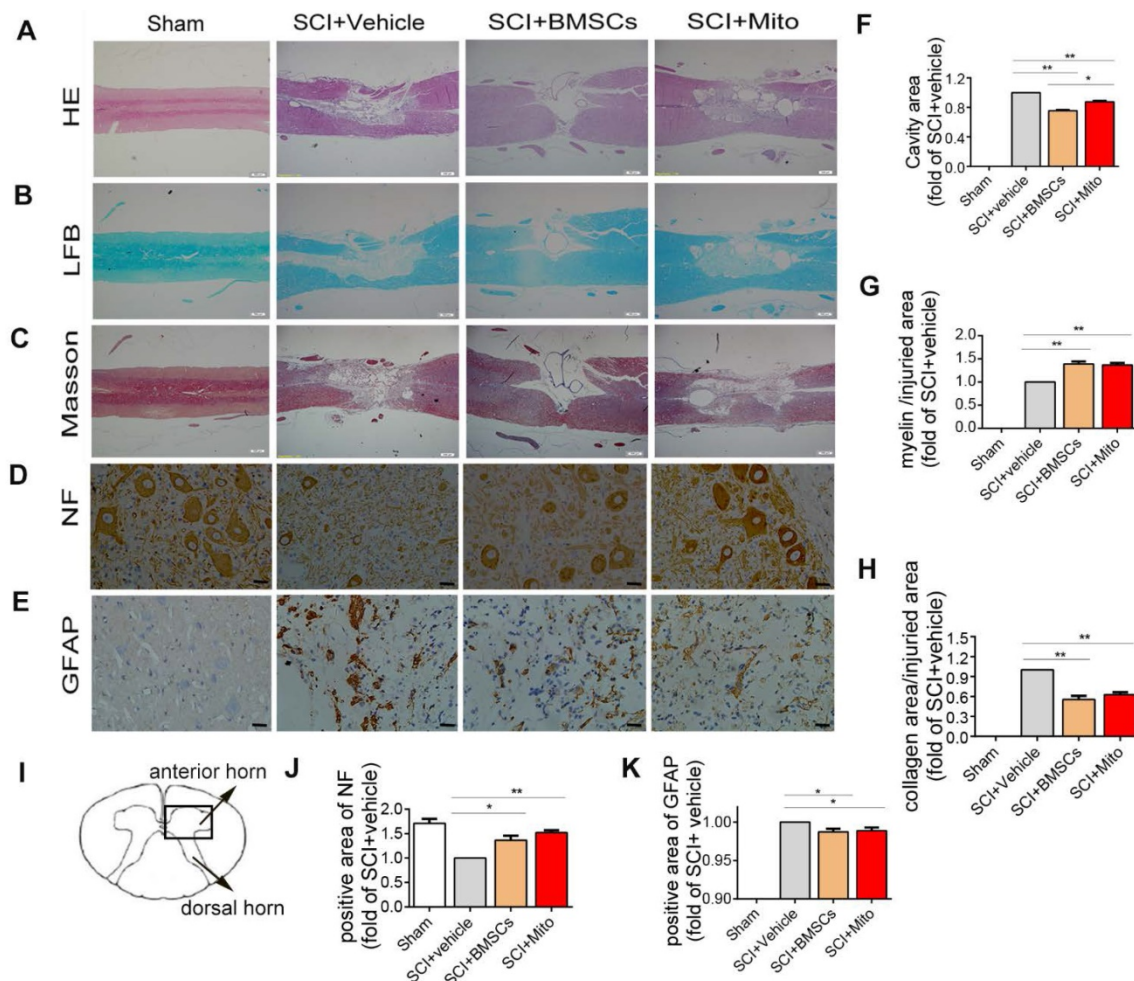


Figure 9. H&E staining, LFB staining, Masson staining and immunocytochemistry staining of spinal cord at 6-week after SCI. (A-C) The longitudinal sections of spinal cord were analyzed by H&E staining, Luxol fast blue staining, Masson staining. Scale bar: 500 μ m; (D-E) Immunohistochemistry assay was performed to detect NF and GFAP positive cells in transverse sections of spinal cord. Scale bar: 25 μ m; (I) Schematic diagram of spinal cord. The areas of lesion cavity (F), myelin (G), collagen (H), NF-H (J) and GFAP (K) were analyzed by IPP software. Each data point was presented as mean \pm SEM (n=3, *P< 0.05, **P< 0.01).

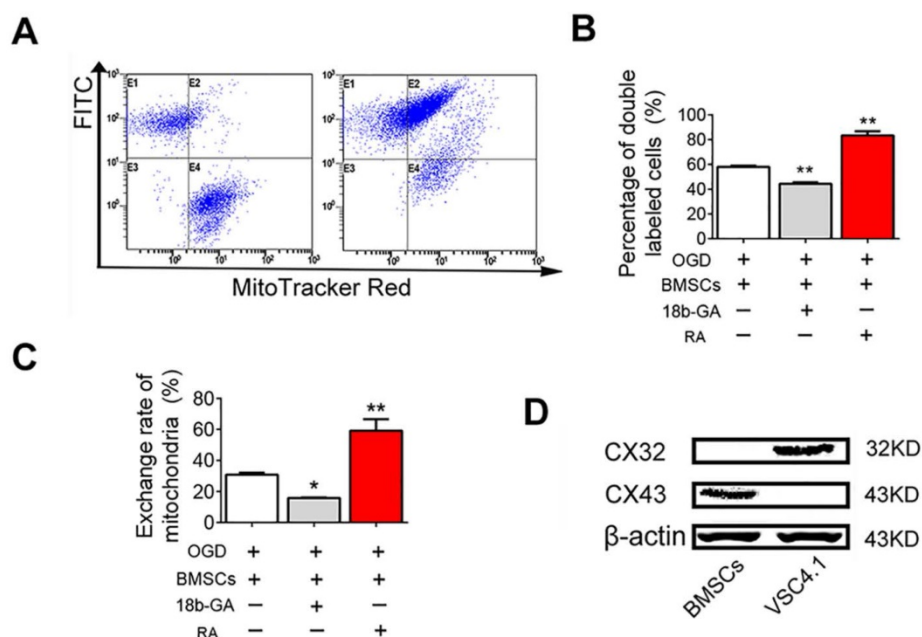


Figure 10. GJIC mediated the mitochondria transfer. (A) FACS was used to detect the exchange of endocytic organelles (including mitochondria) between BMSCs and post-OGD VSC4.1 motor neurons. BMSCs were pre-incubated with GJIC potentiator retinoid acid (RA, 10 μ M) or inhibitor 18 β -GA (50 μ M) for 8 h prior to co-culture. BMSCs were co-cultured with post-OGD VSC4.1 motor neurons for 24 h in a direct co-culture with or without continuous treatment of drugs. (B) Double-positive cells are indicative of organelle transfer cells which means red-labelled mitochondria from BMSCs transferred to green-labelled VSC4.1 motor neurons. (C) The exchange rate of endocytic organelles and mitochondria from BMSCs to VSC4.1 motor neurons was calculated based on the primary data of FACS. (D) The expression levels of connexin43 and connexin32 were detected by western blot analysis in BMSCs or VSC4.1 motor neurons. β -actin was loaded as internal control. Each data point was presented as mean \pm SEM (n=3, *P< 0.05, **P<0.01).

Our results proved that the GJIC is involved in mitochondrial transport between BMSCs and motor neurons, which contributed to rescuing injured neurons from SCI induced apoptosis. Moreover, we also found that astrocyte could uptake BMSCs derived mitochondria. Astrocytes are multifunctional cells which can both exert beneficial and detrimental effect as they can form glial scar to protect healthy tissues from neurotoxic environments, help maintain the blood-brain barrier as well as secrete axonal growth factors. While the activation of astrocytes lead to glial scars and the deposit of chondroitin sulphate proteoglycans which contribute to the negative effects [53, 54]. The effect of BMSCs derived mitochondria on astrocytes activation was worth to be further explored. Furthermore, we could not neglect the effect of BMSCs derived mitochondria on invading macrophage because they uptake mitochondria too. Usually, macrophages can phagocytose exogenous cells and activate inflammation [55]. Whether internalization of BMSCs derived mitochondria can regulate the plasticity of macrophages by promoting the shift of macrophage from M1 to M2 type in SCI rats. It needs attention and further investigation.

In addition, some theoretical questions are raised ahead: Which signaling molecule and signaling pathway trigger the mitochondrial release from BMSCs? What are the fates of these exogenous mitochondria in injured neurons within weeks *in*

in vivo? Meanwhile, there are some technical challenges for the use of BMSCs derived mitochondria for clinical treatment. For example, how to improve the isolation technique to acquire high-quality active intact mitochondria for therapeutic purposes? Which approach of mitochondria transplantation into individuals should be selected, from intravenous or local injection?

In conclusion, we demonstrated that mitochondrial transfer from BMSCs to the injured motor neurons via gap junction. Internalization of mitochondria improved the bioenergetics profile, decreased apoptosis and promoted cell survival in post-OGD motor neurons. It would be one of the effective mechanisms of BMSCs preventing the spinal cord from severe injury in the early stage, which subsequently improved the repair and regeneration in the late stage of SCI. Our findings suggested a future interventional strategy of mitochondria transfer for the patients with SCI.

Abbreviations

SCI: spinal cord injury; BMSCs: bone marrow mesenchymal stem cells; ATP: adenosine triphosphate; OGD: oxygen glucose deprivation; GJIC: gap junctional intercellular communication; FACS: fluorescence-activated cell sorting; RA: retinoid acid; 18 β -GA: 18 β glycyrrhetic acid; OCR: oxygen consumption rates; ECAR: extracellular acidification rate; BBB:

Basso, Beattie and Bresnahan; LFB: Luxol fast blue; DAPI: 2-(4-Amidinophenyl)-6-indolecarbamidine dihydrochloride; TUNEL: terminal deoxynucleotidyl transferase dUTP nick end labelling.

Supplementary Material

Supplementary figures.

<http://www.thno.org/v09p2017s1.pdf>

Acknowledgements

This study was supported by the National Natural Science Foundation of China (No. 81572229 Linlin Wang, 81871845 Xiaoming Zhang, 81371953 Linlin Wang, and 81401011 Tengfei Zhao). Thanks for the technical support provided by the core facilities, Zhejiang university school of medicine, especially the fluorescence-activated cell sorting (FACS) provided by Xinghui Song.

Competing Interests

The authors have declared that no competing interest exists.

References

- Surey S, Berry M, Logan A, Bicknell R, Ahmed Z. Differential cavitation, angiogenesis and wound-healing responses in injured mouse and rat spinal cords. *Neuroscience*. 2014; 275: 62-80.
- Fan B, Wei Z, Yao X, Shi G, Cheng X, Zhou X, et al. Microenvironment Imbalance of Spinal Cord Injury. *Cell Transplant*. 2018; 27: 853-66.
- Fatima G, Sharma VP, Das SK, Mahdi AA. Oxidative stress and antioxidative parameters in patients with spinal cord injury: implications in the pathogenesis of disease. *Spinal Cord*. 2015; 53: 3-6.
- Pu Y, Meng K, Gu C, Wang L, Zhang X. Thrombospondin-1 modified bone marrow mesenchymal stem cells (BMSCs) promote neurite outgrowth and functional recovery in rats with spinal cord injury. *Oncotarget*. 2017; 8: 96276-89.
- Holmes D. Spinal-cord injury: spurring regrowth. *Nature*. 2017; 552: S49.
- Richards C, MacKenzie N, Roberts S, Escorpizo R. People with Spinal Cord Injury in the United States. *Am J Phys Med Rehabil*. 2017; 96: S124-56.
- Lin L, Lin H, Bai S, Zheng L, Zhang X. Bone marrow mesenchymal stem cells (BMSCs) improved functional recovery of spinal cord injury partly by promoting axonal regeneration. *Neurochem Int*. 2018; 115: 80-4.
- Zhao H, Cheng L, Du X, Hou Y, Liu Y, Cui Z, et al. Transplantation of Cerebral Dopamine Neurotrophic Factor Transduced BMSCs in Contusion Spinal Cord Injury of Rats: Promotion of Nerve Regeneration by Alleviating Neuroinflammation. *Mol Neurobiol*. 2016; 53: 187-99.
- Peng RJ, Jiang B, Ding XP, Huang H, Liao YW, Peng G, et al. Effect of TNF- α Inhibition on Bone Marrow-Derived Mesenchymal Stem Cells in Neurological Function Recovery after Spinal Cord Injury via the Wnt Signaling Pathway in a Rat Model. *Cell Physiol Biochem*. 2017; 42: 743-52.
- Ock SA, Baregundi Subbarao R, Lee YM, Lee JH, Jeon RH, Lee SL, et al. Comparison of Immunomodulation Properties of Porcine Mesenchymal Stromal/Stem Cells Derived from the Bone Marrow, Adipose Tissue, and Dermal Skin Tissue. *Stem Cells Int*. 2016; 2016: 9581350.
- Ruzicka J, Machova-Urdzikova L, Gillick J, Amemori T, Romanyuk N, Karova K, et al. A Comparative Study of Three Different Types of Stem Cells for Treatment of Rat Spinal Cord Injury. *Cell Transplant*. 2017; 26: 585-603.
- Tsumuraya T, Ohtaki H, Song D, Sato A, Watanabe J, Hiraizumi Y, et al. Human mesenchymal stem/stromal cells suppress spinal inflammation in mice with contribution of pituitary adenylate cyclase-activating polypeptide (PACAP). *J Neuroinflammation*. 2015; 12: 35.
- Cowan DB, Yao R, Thedsanamoorthy JK, Zurakowski D, Del Nido PJ, McCully JD. Transit and integration of extracellular mitochondria in human heart cells. *Sci Rep*. 2017; 7: 17450.
- Li G, Jia Z, Cao Y, Wang Y, Li H, Zhang Z, et al. Mitochondrial Division Inhibitor 1 Ameliorates Mitochondrial Injury, Apoptosis, and Motor Dysfunction After Acute Spinal Cord Injury in Rats. *Neurochem Res*. 2015; 40: 1379-92.
- Wang Y, Wang J, Yang H, Zhou J, Feng X, Wang H, et al. Necrostatin-1 mitigates mitochondrial dysfunction post-spinal cord injury. *Neuroscience*. 2015; 289: 224-32.
- Jia ZQ, Li SQ, Qiao WQ, Xu WZ, Xing JW, Liu JT, et al. Ebselen protects mitochondrial function and oxidative stress while inhibiting the mitochondrial apoptosis pathway after acute spinal cord injury. *Neurosci Lett*. 2018; 678: 110-7.
- Pandya JD, Nukala VN, Sullivan PG. Concentration dependent effect of calcium on brain mitochondrial bioenergetics and oxidative stress parameters. *Front Neuroenergetics*. 2013; 5: 10.
- Visavadiya NP, Patel SP, VanRooyen JL, Sullivan PG, Rabchevsky AG. Cellular and subcellular oxidative stress parameters following severe spinal cord injury. *Redox Biol*. 2016; 8: 59-67.
- Semple BD. Early preservation of mitochondrial bioenergetics supports both structural and functional recovery after neurotrauma. *Exp Neurol*. 2014; 261: 291-7.
- Troulinaki K, Bano D. Mitochondrial deficiency: a double-edged sword for aging and neurodegeneration. *Front Genet*. 2012; 3: 244.
- Gollihue JL, Rabchevsky AG. Prospects for therapeutic mitochondrial transplantation. *Mitochondrion*. 2017; 35: 70-9.
- Hayakawa K, Esposito E, Wang X, Terasaki Y, Liu Y, Xing C, et al. Transfer of mitochondria from astrocytes to neurons after stroke. *Nature*. 2016; 535: 551-5.
- Hsu YC, Wu YT, Yu TH, Wei YH. Mitochondria in mesenchymal stem cell biology and cell therapy: From cellular differentiation to mitochondrial transfer. *Semin Cell Dev Biol*. 2016; 52: 119-31.
- Islam MN, Das SR, Emin MT, Wei M, Sun L, Westphalen K, et al. Mitochondrial transfer from bone-marrow-derived stromal cells to pulmonary alveoli protects against acute lung injury. *Nature medicine*. 2012; 18: 759-65.
- Hayakawa K, Esposito E, Wang X, Terasaki Y, Liu Y, Xing C, et al. Corrigendum: Transfer of mitochondria from astrocytes to neurons after stroke. *Nature*. 2016; 539: 123.
- Liu W, Ding Y, Zhang X, Wang L. Bone marrow stromal cells inhibit caspase-12 expression in rats with spinal cord injury. *Exp Ther Med*. 2013; 6: 671-4.
- Gu C, Li H, Wang C, Song X, Ding Y, Zheng M, et al. Bone marrow mesenchymal stem cells decrease CHOP expression and neuronal apoptosis after spinal cord injury. *Neurosci Lett*. 2017; 636: 282-9.
- Das A, Wallace Gt, Reiter RJ, Varma AK, Ray SK, Banik NL. Overexpression of melatonin membrane receptors increases calcium-binding proteins and protects VSC4.1 motoneurons from glutamate toxicity through multiple mechanisms. *J Pineal Res*. 2013; 54: 58-68.
- Rambold AS, Kostecky B, Elia N, Lippincott-Schwartz J. Tubular network formation protects mitochondria from autophagosomal degradation during nutrient starvation. *Proc Natl Acad Sci U S A*. 2011; 108: 10190-5.
- Gollihue JL, Patel SP, Eldahan KC, Cox DH, Donahue RR, Taylor BK, et al. Effects of Mitochondrial Transplantation on Bioenergetics, Cellular Incorporation, and Functional Recovery after Spinal Cord Injury. *J Neurotrauma*. 2018.
- Patel SP, Sullivan PG, Pandya JD, Goldstein GA, VanRooyen JL, Yonutas HM, et al. N-acetylcysteine amide preserves mitochondrial bioenergetics and improves functional recovery following spinal trauma. *Exp Neurol*. 2014; 257: 95-105.
- Li Y, Ye Z, Lai W, Rao J, Huang W, Zhang X, et al. Activation of Sirtuin 3 by Silybin Attenuates Mitochondrial Dysfunction in Cisplatin-induced Acute Kidney Injury. *Front Pharmacol*. 2017; 8: 178.
- Weng Y, Chen F, Liu Y, Zhao Q, Chen R, Pan X, et al. *Pseudomonas aeruginosa* Enolase Influences Bacterial Tolerance to Oxidative Stresses and Virulence. *Front Microbiol*. 2016; 7: 1999.
- Wang J, Li H, Yao Y, Ren Y, Lin J, Hu J, et al. beta-Element Enhances GAP-43 Expression and Neurite Outgrowth by Inhibiting RhoA Kinase Activation in Rats with Spinal Cord Injury. *Neuroscience*. 2018; 383: 12-21.
- Zhang E, Yin S, Song X, Fan L, Hu H. Glycoumarin inhibits hepatocyte lipoapoptosis through activation of autophagy and inhibition of ER stress/GSK-3-mediated mitochondrial pathway. *Sci Rep*. 2016; 6: 38138.
- Wang C, Shi D, Song X, Chen Y, Wang L, Zhang X. Calpain inhibitor attenuates ER stress-induced apoptosis in injured spinal cord after bone mesenchymal stem cells transplantation. *Neurochem Int*. 2016; 97: 15-25.
- Fan L, Liu C, Chen X, Zou Y, Zhou Z, Lin C, et al. Directing Induced Pluripotent Stem Cell Derived Neural Stem Cell Fate with a Three-Dimensional Biomimetic Hydrogel for Spinal Cord Injury Repair. *ACS Appl Mater Interfaces*. 2018; 10: 17742-55.
- Guan X, Wilson S, Schlender KK, Ruch RJ. Gap-junction disassembly and connexin 43 dephosphorylation induced by 18 beta-glycyrrhetic acid. *Mol Carcinog*. 1996; 16: 157-64.
- Wu J, Taylor RN, Sidell N. Retinoic acid regulates gap junction intercellular communication in human endometrial stromal cells through modulation of the phosphorylation status of connexin 43. *J Cell Physiol*. 2013; 228: 903-10.
- Ahuja CS, Wilson JR, Nori S, Kottler MRN, Druschel C, Curt A, et al. Traumatic spinal cord injury. *Nat Rev Dis Primers*. 2017; 3: 17018.
- Francois-Quijorna I, Santos-Nogueira E, Gronert K, Sullivan AB, Kopp MA, Brommer B, et al. Maresin 1 Promotes Inflammatory Resolution, Neuroprotection, and Functional Neurological Recovery After Spinal Cord Injury. *J Neurosci*. 2017; 37: 11731-43.
- Hu W, Wang H, Liu Z, Liu Y, Wang R, Luo X, et al. Neuroprotective effects of lycopene in spinal cord injury in rats via antioxidative and anti-apoptotic pathway. *Neurosci Lett*. 2017; 642: 107-12.

43. Bartus K, Galino J, James ND, Hernandez-Miranda LR, Dawes JM, Fricker FR, et al. Neuregulin-1 controls an endogenous repair mechanism after spinal cord injury. *Brain*. 2016; 139: 1394-416.
44. Zhu LL, Li MQ, He F, Zhou SB, Jiang W. Mitochondria Targeted Peptide Attenuates Mitochondrial Dysfunction, Controls Inflammation and Protects Against Spinal Cord Injury-Induced Lung Injury. *Cell Physiol Biochem*. 2017; 44: 388-400.
45. Scholpa NE, Schnellmann RG. Mitochondrial-Based Therapeutics for the Treatment of Spinal Cord Injury: Mitochondrial Biogenesis as a Potential Pharmacological Target. *J Pharmacol Exp Ther*. 2017; 363: 303-13.
46. Mehta A, Prabhakar M, Kumar P, Deshmukh R, Sharma PL. Excitotoxicity: bridge to various triggers in neurodegenerative disorders. *Eur J Pharmacol*. 2013; 698: 6-18.
47. Marlein CR, Zaitseva L, Piddock RE, Robinson SD, Edwards DR, Shafat MS, et al. NADPH oxidase-2 derived superoxide drives mitochondrial transfer from bone marrow stromal cells to leukemic blasts. *Blood*. 2017; 130: 1649-60.
48. Jackson MV, Morrison TJ, Doherty DF, McAuley DF, Matthay MA, Kissenpfennig A, et al. Mitochondrial Transfer via Tunneling Nanotubes is an Important Mechanism by Which Mesenchymal Stem Cells Enhance Macrophage Phagocytosis in the In Vitro and In Vivo Models of ARDS. *Stem Cells*. 2016; 34: 2210-23.
49. Wang L, Zhou JB, Wang X, Wang ZH, Zhao RS. Simultaneous determination of copper, cobalt, and mercury ions in water samples by solid-phase extraction using carbon nanotube sponges as adsorbent after chelating with sodium diethyldithiocarbamate prior to high performance liquid chromatography. *Anal Bioanal Chem*. 2016; 408: 4445-53.
50. Pai CL, Chen YC, Hsu CY, Su HL, Lai PS. Carbon Nanotube-Mediated Photothermal Disruption of Endosomes/Lysosomes Reverses Doxorubicin Resistance in MCF-7/ADR Cells. *J Biomed Nanotechnol*. 2016; 12: 619-29.
51. Sinclair KA, Yerkovich ST, Hopkins PM, Chambers DC. Characterization of intercellular communication and mitochondrial donation by mesenchymal stromal cells derived from the human lung. *Stem Cell Res Ther*. 2016; 7: 91.
52. Jiang D, Gao F, Zhang Y, Wong DS, Li Q, Tse HF, et al. Mitochondrial transfer of mesenchymal stem cells effectively protects corneal epithelial cells from mitochondrial damage. *Cell Death Dis*. 2016; 7: e2467.
53. Tanie Y, Tanabe N, Kuboyama T, Tohda C. Extracellular Neuroleukin Enhances Neuroleukin Secretion From Astrocytes and Promotes Axonal Growth in vitro and in vivo. *Front Pharmacol*. 2018; 9: 1228.
54. Markiewicz I, Lukomska B. The role of astrocytes in the physiology and pathology of the central nervous system. *Acta Neurobiol Exp (Wars)*. 2006; 66: 343-58.
55. Schwartz M. Macrophages and microglia in central nervous system injury: are they helpful or harmful? *J Cereb Blood Flow Metab*. 2003; 23: 385-94.